AGU PUBLICATIONS

JGR

Journal of Geophysical Research: Solid Earth

RESEARCH ARTICLE

10.1002/2013JB010628

Key Points:
- Use seismic array data to analyze LPs and tremor at Arenal volcano in 2004
- Discuss the intriguing differences between the wavefield of LPs and tremor
- Propose a model to explain them in terms of source position and extent

Correspondence to:
J. Almendros,
alm@iag.ugr.es

Citation:
Almendros, J., R. Abella, M. M. Mora, and P. Lesage (2014), Array analysis of the seismic wavefield of long-period events and volcanic tremor at Arenal volcano, Costa Rica, *J. Geophys. Res. Solid Earth*, *119*, 5536–5559, doi:10.1002/2013JB010628.

Received 27 AUG 2013
Accepted 30 MAY 2014
Accepted article online 6 JUN 2014
Published online 2 JUL 2014

Array analysis of the seismic wavefield of long-period events and volcanic tremor at Arenal volcano, Costa Rica

Javier Almendros[1,2], Rafael Abella[3], Mauricio M. Mora[4,5], and Philippe Lesage[6]

[1]Instituto Andaluz de Geofísica, Universidad de Granada, Granada, Spain, [2]Departamento de Física Teórica y del Cosmos, Universidad de Granada, Granada, Spain, [3]Observatorio Geofísico Central, Instituto Geográfico Nacional, Madrid, Spain, [4]Escuela Centroamericana de Geología, Universidad de Costa Rica, San José, Costa Rica, [5]Red Sismológica Nacional (RSN: UCR-ICE), San José, Costa Rica, [6]ISTerre, Université de Savoie, CNRS, Le Bourget-du-Lac, France

Abstract We use wavefield decomposition methods (time domain cross correlation and frequency domain multiple-signal classification) to analyze seismic data recorded by a dense, small-aperture array located 2 km West of Arenal volcano, Costa Rica, and operated during 2.5 days. The recorded wavefield is dominated by harmonic tremor and includes also spasmodic tremor and long-period (LP) events. We find that the initial stages of LP events are characterized by three different wave arrivals. These arrivals propagate with similar back azimuths pointing to the volcano summit (~80°N) and increasing apparent slowness of 0.4, 1.1, and 1.7 s/km. Spasmodic tremors cannot be regarded as coherent signals. On the contrary, harmonic tremors are highly coherent, characterized by the stability of the apparent slowness vector estimates. Apparent slowness lays in the range 1–2 s/km. Back azimuths point in the general direction of the volcano but with a large variability (40–120°N). Nevertheless, there are long-term variations and evidences of multiple simultaneous components in the harmonic tremor wavefield. These observations suggest that LP events and tremor are generated in a shallow source area near the volcano summit, although they do not share exactly the same source region or source processes. The tremor source is located in the shallowest part of the plumbing system, beneath the lava crust. This dynamic region is subject to complex fluctuations of the physical conditions. Degassing events at different locations of this region might generate variable seismic radiation patterns. The effects of topography and heterogeneous shallow structure of the volcano may amplify these variations and produce the wide directional span observed for volcanic tremor. On the other hand, the LP source seems to be more repeatable. LP events are likely triggered by fragmentation of the fluid flow in a slightly deeper portion of the volcanic conduits.

1. Introduction

Arenal volcano is a small stratovolcano (1750 m above sea level (asl)) located in northwestern Costa Rica (Figure 1). It remained eruptive for 42 years, from 1968, when a magmatic andesitic eruption took place after centuries of dormancy [*Alvarado et al.*, 2006], until 2010, when lava effusion gradually stopped. This long-lasting eruption went through different stages set by changes on explosive and effusive activity.

The eruption of 29 July 1968 opened three new craters named A, B, and C, from lower to upper [*Melson and Saenz*, 1968; *Minakami et al.*, 1969]. During the next few years, basaltic-andesitic lavas were effused from crater A located at 1050 m asl [*Wadge et al.*, 2006]. In 1974, the activity shifted to crater C at ~1400 m asl on the western flank of the edifice [*Wadge et al.*, 2006], as shown in Figure 2 (left). 'A'ā lava flows were erupted almost continuously [*Borgia and Linneman*, 1980; *Wadge*, 1983] and a new cone developed [*Cigolini et al.*, 1984; *Alvarado and Soto*, 2002]. The new cone grew and a lava pool was set up (Figure 2 (center)). Strombolian activity began in 1984 [*Borgia et al.*, 1988; *Barquero et al.*, 1992; *Williams-Jones et al.*, 2001]. In 1987, it changed to Vulcanian eruptions that recurrently destroyed the crust that used to be at the top of the lava lake. The explosive activity was accompanied with infrequent pyroclastic flows originating from column collapse, lava front collapse, and lava pool collapse [*Alvarado and Arroyo*, 2000; *Alvarado and Soto*, 2002]. After 1998, there was a marked decrease in explosive activity, from rates of tens of daily explosions to ~5 or less explosions per day [e.g., *Cole et al.*, 2005]. This happened at the same time that Arenal effusive rate fell from ~2 m^3/s in the 1980s to 0.1–0.2 m^3/s in 2004 [*Wadge et al.*, 2006]. The lava pool became a viscous and degassed lava crust with dome-like structures leading to short lava flows (Figure 2 (right)). Afterward, Arenal eruptive activity was mainly effusive with infrequent explosions [*Wadge et al.*, 2006]. The volcanic

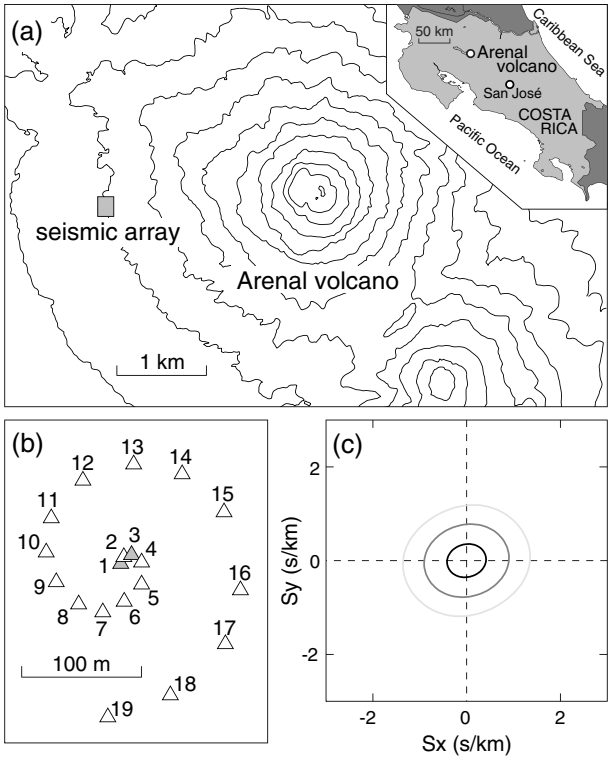

Figure 1. (a) Location of the seismic array about 2 km west of the Arenal volcano summit. The gray box indicates the array location and corresponds to the area zoomed in Figure 1b. The inset shows the location of Arenal volcano in Costa Rica. (b) Configuration of the seismic array. Grey triangles indicate stations that were partially disregarded for this study. (c) Beam-forming array response at 2.5 Hz. We show contours of 30, 60, and 90% of the maximum.

activity practically ceased in October 2010, and nowadays, it remains only as a tenuous degassing. Along the eruption the point of effusion was raised about 250 m from 1974 until 2005 [*Wadge et al.*, 2006] and grew more that 35 m afterward [*Alvarado*, 2011], reaching 1750 m asl approximately at the ceasing of the volcanic activity.

Seismic activity accompanying the eruption at Arenal until 2010 was characterized by a large variety of signals including harmonic and spasmodic tremors, explosion quakes, LP events, rockfall events, and volcano-tectonic swarms [*Alvarado et al.*, 1997]. Tremors, particularly the harmonic type, and explosion quakes have been the subject of several studies [*Alvarado and Barquero*, 1987; *Barquero et al.*, 1992; *Alvarado et al.*, 1997; *Benoit and McNutt*, 1997; *Hagerty et al.*, 2000; *Metaxian et al.*, 2002; *Mora*, 2003; *Lesage et al.*, 2006; *Davi et al.*, 2010, 2012; *Almendros et al.*, 2012], leading to achieve important advances on the understanding of the source processes. However, although several source models have been considered, none of them can account for all the features of the seismic signals. More complex has been to match those features to the observations of the volcanic activity and geological context.

Harmonic tremor was the most conspicuous signal at Arenal, usually lasting several hours per day. Harmonic tremor spectra contained several regularly spaced peaks at integer multiples of the fundamental frequency which was generally in the range 0.9–2 Hz [*Hagerty et al.*, 2000; *Mora*, 2003; *Lesage et al.*, 2006]. Time-frequency analysis of continuous records reveals large variations (>50%) of the fundamental frequency in periods of minutes to tens of minutes [*Benoit and McNutt*, 1997; *Hagerty et al.*, 2000; *Mora*, 2003]. Spasmodic tremor was characterized by energy distributed in a wide frequency band, usually in the range 1–6 Hz. Explosion quakes were also quite common, although their number and intensity decreased in the last 10 years of the eruption. Strong explosions were often accompanied by a large audible boom [*Alvarado and Barquero*, 1987; *Barquero et al.*, 1992; *Garces et al.*, 1998] producing a high-frequency seismic phase several seconds after the *P* wave onset, due to coupling between the acoustic waves and the ground. The explosion coda frequently became harmonic tremor [*Barquero et al.*, 1992; *Benoit and McNutt*, 1997; *Hagerty et al.*, 2000; *Mora*, 2003]. LP events were very similar to explosion quakes except that their records had smaller amplitudes and did not display acoustic phases. *Lesage et al.* [2006] proposed that LP events and explosion quakes could be considered as part of the same type of event, as there is probably no fundamental difference in their mechanism. In the late 1990s, tens to hundreds of these events were observed each day [*Mora*, 2003]. The seismic sources of tremor and discrete events were located below the active crater [*Alvarado et al.*, 1997; *Hagerty et al.*, 2000; *Metaxian et al.*, 2002; *Davi et al.*, 2010, 2012]. Finally, several volcano-tectonic swarms were usually detected a few months before the major pyroclastic flows originated by crater wall collapses [*Alvarado and Arroyo*, 2000; *Alvarado and Soto*, 2002]. Other volcano-tectonic swarms were detected during the last stages of the eruption and after the end of volcanic activity.

In this paper, we perform a detailed analysis of LP event and tremor wavefields using data from a dense, small-aperture seismic array operated in 2004. We address their propagation characteristics using two array

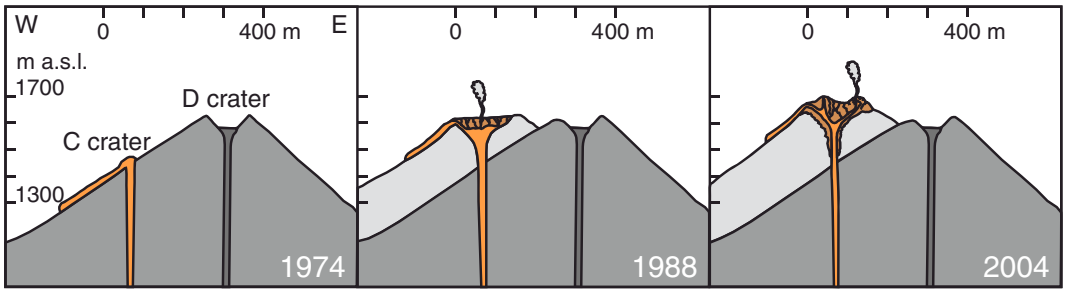

Figure 2. Sketch of the plumbing system under the C crater of Arenal volcano at three stages (1974, 1988, and 2004) during the 1968–2010 eruption. The pre-1968 and post-1968 edifices are shown in dark and light gray, respectively. Fluid magma is represented in orange, while solidified parts are shown in brown.

methods and investigate the similarities and differences in their propagation parameters. We find that LP and tremor wavefields are substantially different, which opposes the widely accepted view of volcanic tremor as a superposition of LP events. We also discuss the detection of multiple simultaneous sources in the seismic wavefield. Our results allow us to propose new insights into the seismic source processes at Arenal volcano, revisiting the interpretation of LP and explosion sources as well as the striking features of harmonic tremors.

2. Instruments and Data

In February 2004 a dense, small-aperture seismic array was deployed during 2.5 days (22 February 01:00 to 24 February 14:00) on the west flank of Arenal volcano, at an elevation of ~700 m. The summit lies at about 2 km from the array in a 85°N direction (Figure 1a). The array was composed by 19 short-period (1 Hz), three-component, Lennartz LE-3Dlite seismometers connected to Reftek 130 data loggers recording at a sampling frequency of 100 sps and synchronized by GPS time. Seismometers were distributed in a spiral configuration (Figure 1b) with an aperture of 210 m. It has been demonstrated that the variety of interstation distances that characterizes this configuration reduces the impact of spatial aliasing (S. Gaffet, personal communication, 2003) and generally favors the quality of the array response (Figure 1c).

The seismic data recorded during the 60 h of array operations reflect the continuous character of the volcanic activity at Arenal volcano during the experiment. Although the level of explosions and tremor activity showed a large variability during the eruption, the main spectral features remained similar over time, making the data set from this short-term experiment quite representative of the overall seismicity of Arenal volcano. The data contain several (~200) LP events and two types of volcanic tremor (harmonic and spasmodic). Harmonic tremor is the most conspicuous signal, comprising a total of 43 h. On the other hand, spasmodic tremor episodes last for a total of 12 h, part of them overlapped with harmonic tremors. Figures 3 and 4 show examples of the waveforms and spectral contents of these types of signals. Figure 5 shows the temporal distribution of tremors and LP events along the 2.5 days selected for the analysis. The data set contains also a few tectonic earthquakes, but none of them are related to volcanic activity at Arenal.

Tremor and LP events can be associated, generating what has been called by *Benoit and McNutt* [1997] as whooshes and chugs. *Lesage et al.* [2006] found that there are transitions between harmonic and spasmodic tremor, leading them to propose that a common source can be involved on both harmonic and spasmodic tremor generation. They also reported multiple groups of harmonics in tremor spectrograms, which constitute an evidence of simultaneously active sources. Our data contain examples of all these features, such as harmonic tremors with overlapping spectral lines and other evidences of simultaneous sources (Figure 4). In Figure 5 we indicate the temporal extent of this volcanic tremor overlapping.

3. Application of Array Methods

Seismic arrays provide a representation of the propagation of seismic wavefields generated by the volcanic activity. This information can be used both to investigate the peculiarities of the medium and the array sites and to infer the characteristics of the seismogenic processes that occur in volcanoes. Array analyses of volcanic signals have been performed at several volcanic areas such as Kilauea [*Goldstein and Chouet*,

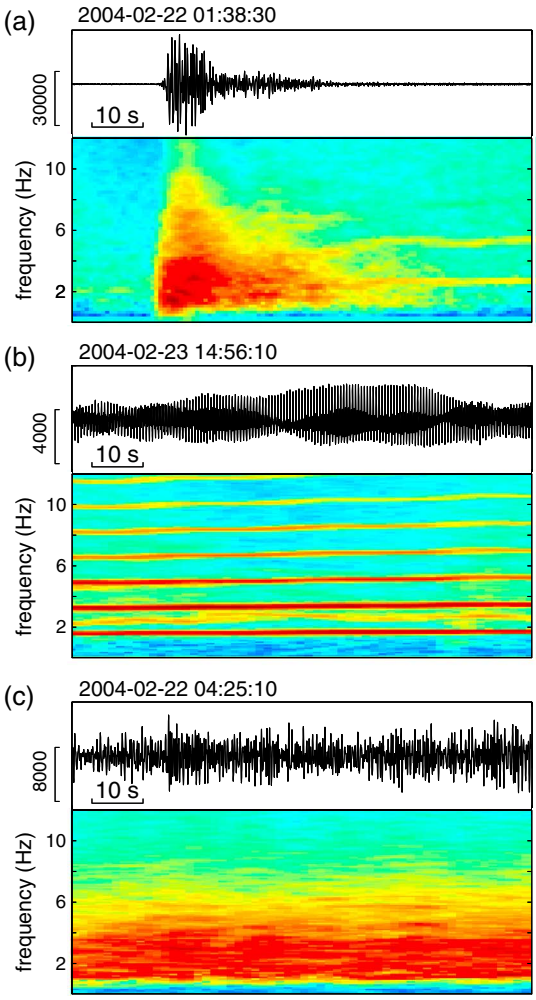

Figure 3. Examples of seismograms and spectrograms of typical seismovolcanic events: (a) LP event, (b) harmonic tremor, and (c) spasmodic tremor.

1994; *Almendros et al.*, 2001b], Stromboli [*Chouet et al.*, 1997; *La Rocca et al.*, 2004], Etna [*Saccorotti et al.*, 2004; *Di Lieto et al.*, 2007], Teide [*Almendros et al.*, 2000, 2007], Colima [*Palo et al.*, 2009], Aso [*Takagi et al.*, 2006], Kirishima [*Matsumoto et al.*, 2013], and Ubinas [*Inza et al.*, 2014]. These analyses are specially useful for volcanic tremor, which constitutes an elusive signal that has to be investigated using unconventional approaches.

We use array processing techniques to estimate time series of the apparent slowness vectors representative of the seismic wavefield at Arenal volcano. In order to understand the procedure, we have to underline that the data we are dealing with have peculiarities that might complicate the array analysis. For example, we enumerate the following:

1. There are transient (LP events) and sustained signals (volcanic tremor). LP events occur as a response to short-lived perturbations at the seismovolcanic source. The duration of the coherent part (i.e., duration of the source) is shorter than the total duration of the signal (few tens of seconds). Conversely, volcanic tremors are the consequence of a sustained excitation. Although they may display slight fluctuations, they maintain a high level of coherence between array stations for long time spans.
2. Harmonic tremor at Arenal is characterized by important temporal variations in frequency. The fundamental frequency of harmonic tremor is often stable; nevertheless, it can change significantly within minutes (frequency gliding [*Lesage et al.*, 2006]). In any case, tremor frequencies are generally restricted to the 1.5–3.5 Hz range. LP events, on the other hand, have a relatively wide band frequency content. Most energy is contained in the 1–4 Hz band, although their spectra may include relevant energy up to 8 Hz.
3. Multiple sources might be acting simultaneously. This is evidenced by superimposed records of LP and tremors. However, the differences in amplitude and character of these signals are generally large and they can be analyzed independently. A more subtle phenomenon is the activation of multiple harmonic tremor sources at the same time, evidenced by independently evolving sets of harmonic lines in the spectrograms.

These peculiarities, specially the last one, constitute a serious challenge for the wavefield analysis capabilities of the seismic array. Therefore, we decided to apply two different array methods based on different approaches. The first one is the zero-lag cross-correlation (ZLCC) technique [*Frankel et al.*, 1991; *Del Pezzo et al.*, 1997]. This is a time domain method that produces highly stable solutions, and within some limits, it can work with any window length and frequency content. It allows for a robust estimate of the apparent slowness vector of the dominant component of the seismic wavefield. The second method is the multiple signal classification (MUSIC) algorithm [*Schmidt*, 1986; *Goldstein and Archuleta*, 1987], a frequency domain technique that stretches the capabilities of array processing in order to enhance resolution in the apparent slowness vector plane. MUSIC is limited by the window length, which controls the resolution in time and frequency, like other spectral methods. Above this limitation, the main advantage is that MUSIC allows

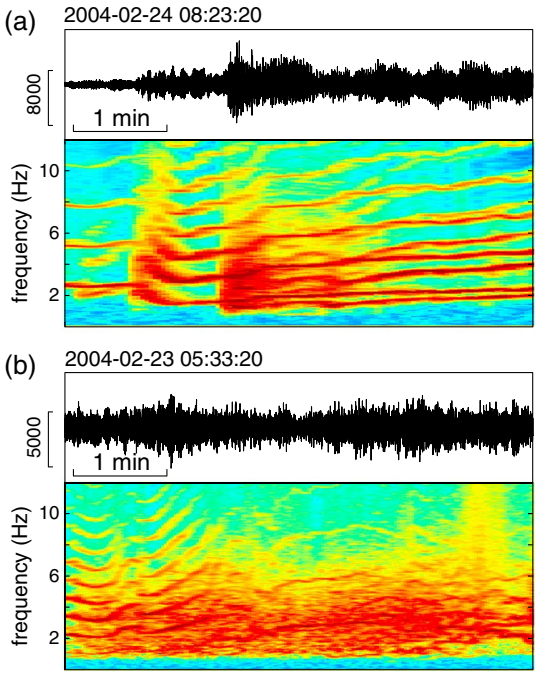

Figure 4. Examples of seismograms and spectrograms revealing double sources: (a) Two simultaneous harmonic tremors and (b) simultaneous harmonic and spasmodic tremors.

for the analysis of complex wavefields containing narrowband signals from several simultaneous sources. In order to make their results comparable and aid in the interpretation, we use both methods with similar parameters.

The next step was to check the completeness and quality (signal-to-noise ratio) of the data set. Station 13 did not work for the first 20 h, and a few more stations were intermittently up and down from 12:00 to 14:00 on 22 February. Thus, we do not use these channels at those periods. We have the 19 channels available for 67% of the time, 18 channels for 30% of the time, and 15–17 channels for the remaining 3%. For the ZLCC calculations, we rule out two extra stations among those that were tightly deployed in the central part of the array. Instruments located closer than the distance traveled by the wavefronts at the slowest pace considered (largest apparent slowness) during a sampling interval do not add information to the problem but result in extra noise and worse array response. This precaution is not necessary in the MUSIC method, which works in the frequency domain. We could have stacked the central channels of the array in order to get a single seismogram with improved signal-to-noise ratio (SNR). But there are a few arguments against this, for example: (1) the SNR is good enough for our purposes; (2) for slow waves, stacking could modify substantially the waveforms, since it implies assuming simultaneous arrivals (very small apparent slowness); and (3) interstation distances grow very gradually and it is not clear what stations should be selected. Therefore, we did not stack the seismograms. This processing would make sense if we had low SNR and a set of dense clusters separated by distances much larger than the cluster sizes, as in some large-aperture seismic arrays [*Gupta et al.*, 1990; *Rost and Thomas*, 2002].

We select the 1–4 Hz band for both analyses. For the ZLCC method, we filter the signals using a zero-phase, two-pole Butterworth filter. For the MUSIC method, we limit the analysis to the spectral values within that range. The low-frequency limit of the frequency band selected is imposed by the instrument response. Although our array is dense enough to make possible the inclusion of frequencies higher than 4 Hz in the analysis, we decided to fix the upper limit to that frequency because of the following reasons: (1) the 1–4 Hz band contains most of the energy of the LP events and tremors; (2) the interpretation of the results is simpler when we deal with long wavelengths; and (3) most array methods, and specially MUSIC, work better with narrowband signals.

We adjust the window length for the analysis according to the duration of the input signals. For LP events we selected a 1.28 s (128 samples) window length in order to obtain a good temporal resolution and independent information for events occurring close in time. In principle there is no limitation on the window length in the ZLCC method, except the recommendation that optimum results for transients are achieved when the window contains two to three cycles at the frequencies of interest [*Almendros et al.*, 1999, 2000]. For the MUSIC method, a trade-off between temporal and spectral resolution has to be achieved. A short window means a sparse spectral representation of the data in the frequency domain. For example, a window of 1.28 s implies that the spectra can be calculated with a frequency interval of 0.78 Hz. Thus, we follow *Goldstein and Archuleta* [1991], who suggested the use of a conservative low-frequency limit of twice the frequency interval, in this case 1.56 Hz. For sustained signals (tremors), we select a window length of 5.12 s (512 samples), which contains about 12 cycles at the central frequency of the band selected. In this way, short-lived transients are averaged and the results reveal mainly the behavior of long-lasting sources. These windows were shifted 0.2 and 0.8 s each step, respectively, to analyze the whole data set.

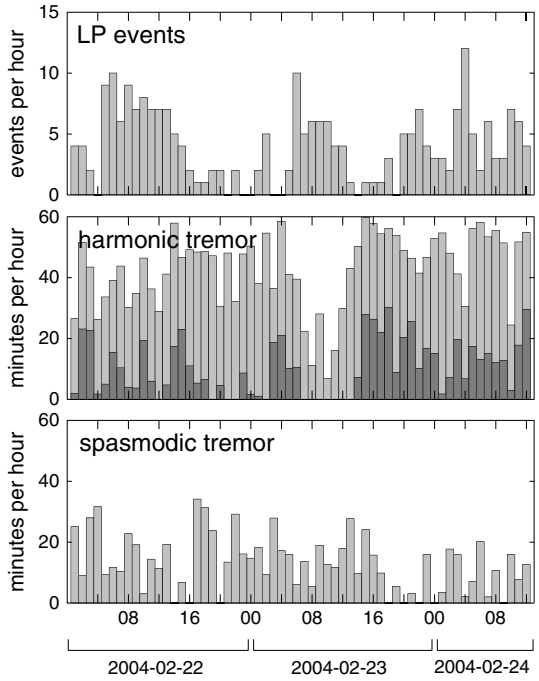

Figure 5. Distribution of seismovolcanic signals along the period analyzed. (a) Hourly number of LP events, (b) minutes of harmonic tremor per hour, and (c) minutes of spasmodic tremor per hour. Dark gray bars in Figure 5b indicate the length of periods with simultaneous sets of independent harmonics.

For each time window, we perform a grid search in the apparent slowness vector space to find the apparent slowness vectors that best represent the propagation properties of the seismic wavefronts. We define an apparent slowness grid from −3.6 to 3.6 s/km in the east and north components of the apparent slowness vector, wide enough to include the expected range of slowness for the signals of interest. The grid spacing was 0.05 s/km, which is adequate to the temporal sampling and configuration of the seismic array. For the ZLCC method, we align the seismograms for each grid node and calculate the array-averaged cross correlation. The apparent slowness vector corresponding to the maximum average cross correlation (MACC) is regarded as our best estimate of the apparent slowness and azimuth of the wavefield contained in the data window. We define an uncertainty region as the area of the apparent slowness domain where the average cross correlations are larger than 90% of the MACC [*Almendros et al.*, 1999]. For well-correlated signals, the size of this area is similar to the beam-forming array response shown in Figure 1c. For the MUSIC method, we calculate the MUSIC power at each grid node. This magnitude represents the inverse of the projection of the signal vector on the noise subspace [*Goldstein and Archuleta*, 1987]. Following *Ueno et al.* [2010], we fix the signal subspace dimension (number of sources) to 3, given that the sum of the three largest eigenvalues of the cross-spectral matrix is always above 95% of the total sum of eigenvalues. The apparent slowness vectors corresponding to local maxima in the MUSIC power distribution are regarded as our best estimates of the apparent slowness and azimuths of the wavefield components contained at each window. The corresponding values of peak MUSIC power (PMUP) indicate the relative strengths of these components.

Altogether, the procedure outlined above leads to time series of (1) apparent slowness and propagation azimuth (together with their uncertainties) and (2) a measure of the quality of the solutions (either MACC or PMUP). These outputs represent the direction, velocity, and relative strength of plane wavefronts propagating across the array that best fit the real wavefield. In order to extract meaningful information from these apparent slowness vector time series, we use the approach of *Almendros et al.* [2001b] and focus on the quality and stability of the solutions. Apparent slowness vector data are averaged in short time windows comprising either a seismic phase within the LP waveform or a stable section of tremor. Our criteria in selecting these windows are (1) a high PMUP, indicative of good coherence between the array traces, and (2) stability in the back azimuth and apparent slowness estimates. In this way, we obtain a single apparent slowness vector estimate for each phase. The total number of estimates is 683 for LP events and 3856 for tremor.

4. Results

4.1. LP Events

Although LP events may display a wide range of amplitudes, the array analysis reveals that most of them have similar characteristics in terms of wave propagation. Figure 6 shows examples of the apparent slowness vector time series during the onset of three LP events of different sizes. We can identify at least three consecutive phases arriving at approximately fixed time intervals. These phases propagate with similar back

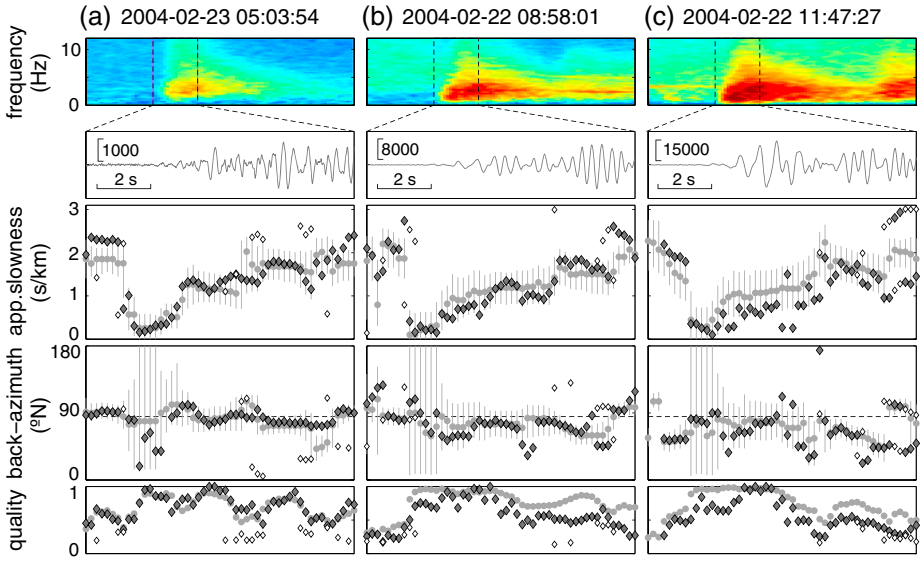

Figure 6. (a–c) Time series of the apparent slowness vector estimates for three LP events. (from top to bottom) Spectrogram, seismogram, apparent slowness, back azimuth, and quality of the estimate (MACC and normalized PMUP). Gray circles show the results of the ZLCC method. Gray and white diamonds correspond to the results of the MUSIC method and represent the dominant and secondary components of the wavefield, respectively. Time labels shown at the top indicate the initial times of the bottom windows (first dashed lines in the spectrograms). Window lengths are 1 min for the top row and 10 s for the remaining rows.

azimuths near 85°N (coming from the volcano summit direction) and increasing apparent slowness. The event coda is initially incoherent, although it very often evolves into a continuous volcanic tremor. This behavior is common to most LP events throughout the data set.

The first arrival is the fastest and faintest. It propagates across the array site with apparent slowness around 0.4 ± 0.2 s/km. Its amplitude is very small compared to the next phases of the LP event, and thus, we very often miss this arrival for events with low SNR. The second phase is the most coherent. It arrives about 1.5 ± 0.5 s after the first onset, with average apparent slowness around 1.1 ± 0.2 s/km. Very often it has a frequency slightly lower than the remaining waveform. Finally, the last phase arrives about 2.9 ± 0.4 s later, generally displaying the largest seismic amplitudes. It is characterized by a large apparent slowness around 1.7 ± 0.1 s/km and lower coherency.

We have not observed a dependence between the apparent slowness vectors, the relative delays of these phases, and the size of the LP events. Furthermore, there are no clear temporal trends either along the time period analyzed.

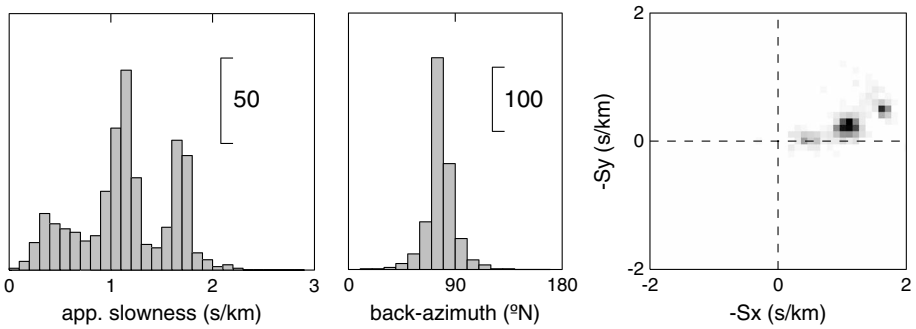

Figure 7. Histograms of the apparent slowness vector results for LP events, obtained using the MUSIC method. (from left to right) Apparent slowness, back azimuth, and 2-D histogram on the apparent slowness vector plane.

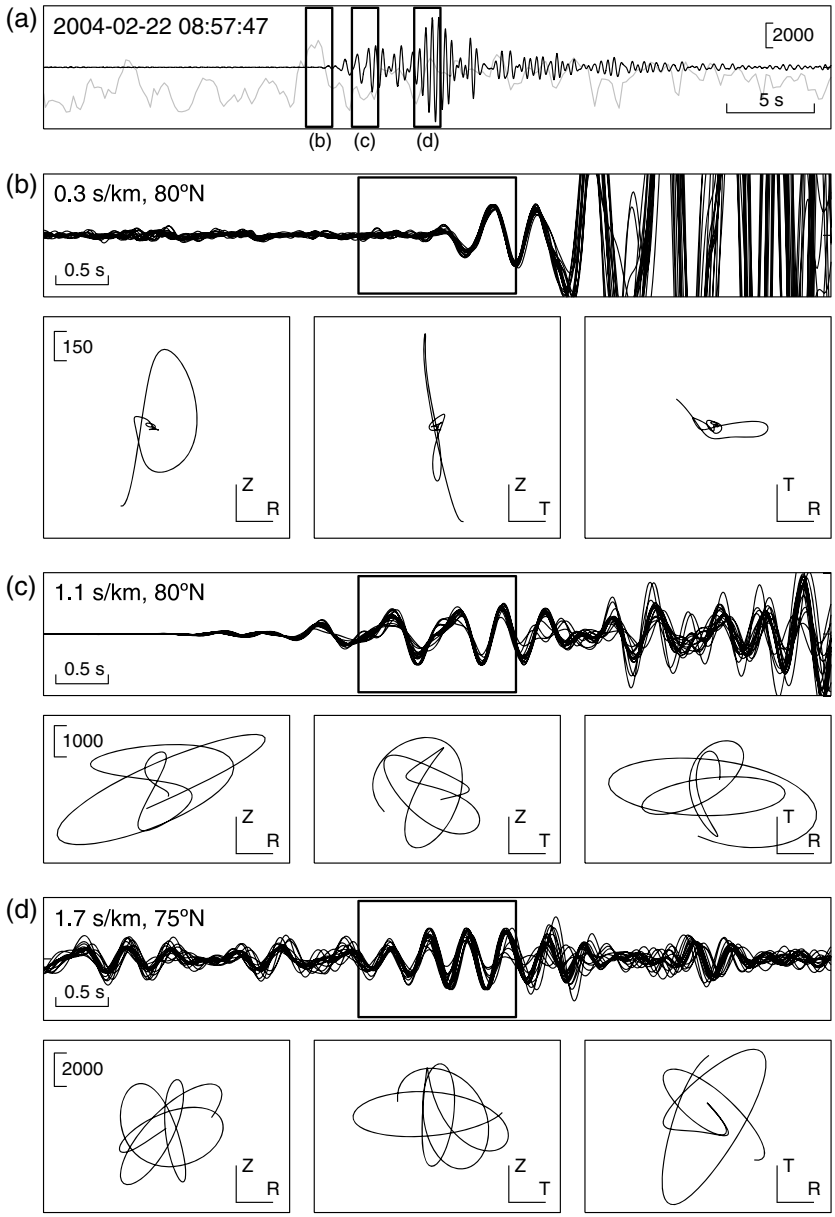

Figure 8. Particle motions for the initial phases of an LP event (shown in Figure 6b). (a) Vertical component seismogram (black line) and rectilinearity (gray line). Rectilinearity scale ranges from 0 at the bottom of the box to 1 at the top. The three boxes indicate the windows zoomed in Figures 8b–8d. (b, top) Seismograms for all array stations for the first window shown in Figure 8a. Traces have been corrected by propagation delays according to the apparent slowness and back azimuth displayed at the top left. (b, bottom) Particle motion projections in the (left) radial vertical, (center) transverse vertical, and (right) radial transverse planes. (c) Same as Figure 8b; for the second window shown in Figure 8a. (d) Same as Figure 8b; for the third window shown in Figure 8a.

Figure 7 shows a summary of the apparent slowness vector estimates obtained using the MUSIC method for all LP events analyzed. The average back azimuth is 80 ± 10°. The three peaks in the apparent slowness distribution at 0.4, 1.1, and 1.7 s/km correspond to the three arrivals described above.

We have performed particle motion analyses of the LP events (Figure 8). Following *Jurkevics* [1988], we correct the array records of propagation delays using the apparent slowness vectors determined by the array analysis. The polarization of the first phase is highly rectilinear. It is contained basically in the incidence plane, with dominant vertical motions. This is fully compatible with a *P* wave propagating with small

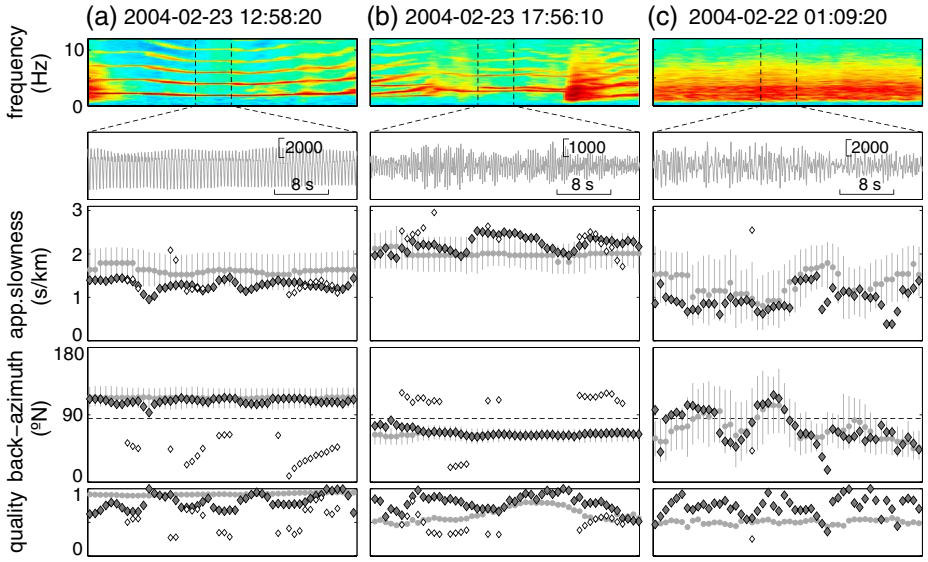

Figure 9. Same as Figure 6 for three samples of volcanic tremor. (a, b) Harmonic tremors and (c) spasmodic tremor. Window lengths are 5 min for the top row and 40 s for the remaining rows.

apparent slowness. The other two phases have a complex particle motion, with significant energy in the transverse component, suggesting the contribution of surface waves.

4.2. Volcanic Tremor

Figure 9 shows examples of the apparent slowness vector time series during harmonic and spasmodic tremor episodes. The array analysis reveals that harmonic tremors are generally coherent and very stable signals. Nevertheless, the back azimuth estimates are quite diverse for tremors along our data set. For example, Figure 9a corresponds to a signal propagating from ~120°N, while Figure 9b displays a signal coming from ~65°N. Spasmodic tremors (Figure 9c) show scattered solutions, with generally low values of MACC/PMUP. In fact, only about 5% of the high-quality solutions identified are clearly related to period dominated by spasmodic tremors. In any case, we have observed that there are no fundamental differences among spasmodic and harmonic tremors in terms of propagation azimuths and apparent slowness.

Particle motions of volcanic tremor are very complex, with strong transverse components indicative of shear motions. Wave polarization of harmonic tremor is particularly intriguing. The trajectories of the particle motions can be very stable during long time periods. They may show elliptical paths, eight-shaped paths, or even more complex figures. Moreover, they display short-wavelength spatial variations, changing sharply within the array stations over distances of ~100 m. The investigation of these features exceeds the purpose of the present article and will be the subject of a separate study that is already in preparation.

When we put together all results for volcanic tremor, we find that seismic waves propagate across the array with similar apparent slowness around 1.5 ± 0.3 s/km. There are small variations, but about 90% of the apparent slowness estimates lay between 1 and 2 s/km (Figure 10). The slow propagation and the complex polarization suggest a dominance of surface waves in the seismic wavefield. Contrarily, we find a significant dispersion in azimuth. This dispersion implies that volcanic tremors may propagate with quite different apparent slowness vectors (i.e., different back azimuths). The average back azimuth for all our tremor estimates is 80°N, which coincides with the back azimuth of the LP events and the direction of the volcano. But there are high-quality estimates of back azimuth in a range of ±40° from that direction, as illustrated in Figures 9a and 9b. For these estimates, uncertainty regions in the apparent slowness plane subtend angles from the origin of less than 30°, which gives an indication of the azimuth resolving capabilities of the seismic array. Definitely, the array has enough azimuthal resolution to differentiate wave arrivals coming from 40 or 120°N. We conclude that the scatter in azimuth is not an effect of the array analysis but a real feature of the volcanic tremor wavefields.

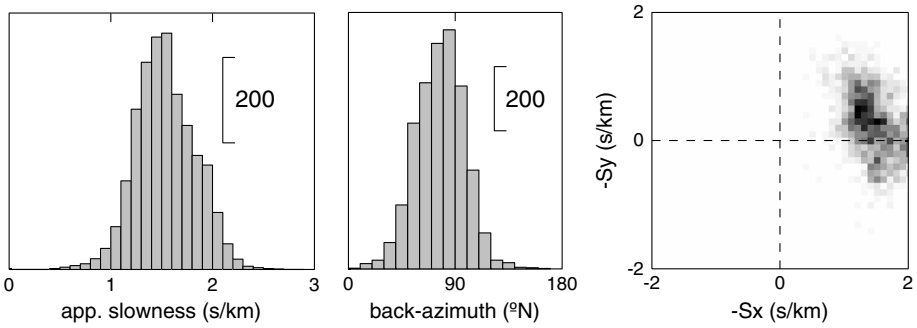

Figure 10. Same as Figure 7 for apparent slowness vector results corresponding to volcanic tremors.

Large variations in back azimuth are produced even within single-tremor episodes displaying apparently continuous waveforms. For example, Figure 11a illustrates a harmonic tremor episode with apparent slowness of ~2 s/km. Around the center of the time window, we witness a smooth change in the back azimuth of the wavefield from 50 to 120°, produced in a time frame of about 10 s. There are no noticeable changes in the frequency of the harmonics. Figure 11b is another example of harmonic tremor, following an LP event, that propagates with apparent slowness of ~1.5 s/km. In this case, we observe a sharp jump in the back azimuth estimates from 120 to 50°. Azimuths both before and after the jump remain stable for more than 20 s. In Figure 11c we see both variation styles in a small time frame of about 20 s. At the beginning of the window the back azimuths are stable at 50°, then they vary smoothly to 120°, and finally they jump back to 50°.

In addition to these temporal variations, we have also found clear evidences of multiple, simultaneous wave components in the seismic wavefield (Figure 12). We are able to detect these episodes thanks to the MUSIC capability to provide independent solutions for the coherent wave components present in the wavefield. These episodes of multiple wave components are always related to harmonic tremors, and last a few tens of seconds. They do not occur during spasmodic tremors or LP events, whose wavefields are characterized well enough by a single wave component. In our application we obtain two solutions corresponding to different apparent slowness vectors. The third signal imposed by our selection of the signal subspace dimension is generally characterized by a small PMUP and has not been considered. The differences in the apparent

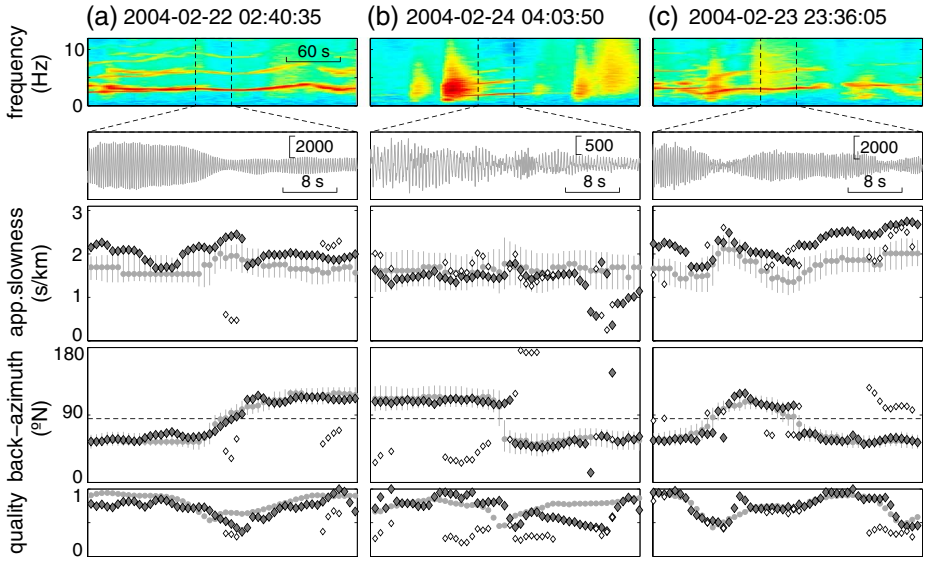

Figure 11. (a–c) Same as Figure 6 for samples of volcanic tremor with a wavefield displaying varying propagation azimuth. Window lengths are 5 min for the top row and 40 s for the remaining rows.

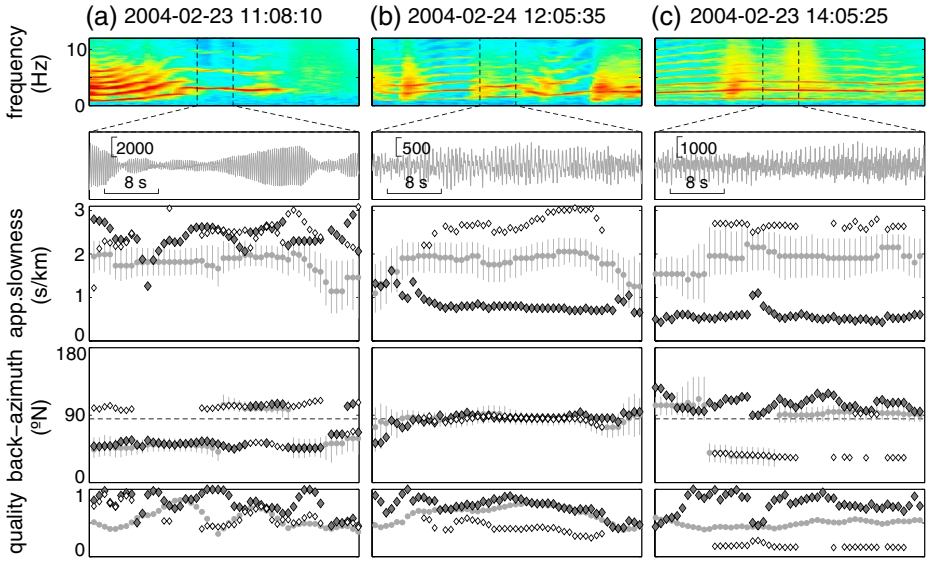

Figure 12. Same as Figure 6 for samples of harmonic tremor showing evidences of a complex wavefield. (a) Two wavefield components at different azimuths, (b) two wavefield components with different apparent slowness, and (c) two wavefield components with both different azimuths and different apparent slowness. Window lengths are 5 min for the top row and 40 s for the remaining rows.

slowness vectors of the solutions can be related to propagation azimuth only (Figure 12a), apparent slowness only (Figure 12b), or both (Figure 12c). During these multiple source episodes, the PMUP of the secondary peak (which indicates the strength of the secondary component in the wavefield) ranges from small values just above noise level to almost the PMUP of the main peak.

Finally, we have not observed any regular trends in the variations of apparent slowness or back azimuth of volcanic tremor with time.

5. Discussion

5.1. Comparison of Methods

We have applied two array methods (ZLCC and MUSIC) based on different approaches. To our knowledge, this is the first time that a systematic comparison of these methods has been attempted. The combination of results helps us reach a better understanding of the wavefield properties. Generally speaking, the propagation azimuths provided by the MUSIC and ZLCC methods coincide, at least within the uncertainty limits of our estimates. On the contrary, the apparent slowness results display slight but systematic variations, specially for harmonic tremors. Figure 13 shows the differences between the back azimuth and apparent slowness values calculated using ZLCC and MUSIC. We include estimates with MACC larger than 0.2 and PMUP over 2, which is not very restrictive (the similarity of results improves when we impose higher thresholds). The azimuth distribution is highly peaked near zero, which indicates that both methods produce basically similar back azimuth estimates, as expected. In fact, about 75% of the solutions present differences within $\pm 15°$, which is about the resolution capability of the array for apparent slowness around 1.5 s/km. The apparent slowness distribution is broader and follows a normal distribution. The standard deviation is 0.45 s/km, which is relatively large compared to the resolution capabilities of the array (Figure 1c). The mean is 0.1 s/km, which indicates that for some reason ZLCC tends to produce apparent slowness estimates systematically larger than MUSIC.

This bias may be due to a methodological difference. ZLCC uses directly apparent slowness to calculate interstation delays and align the seismograms. MUSIC uses wave number instead, which is proportional to the product of apparent slowness and frequency. In this algorithm, the apparent slowness values given as results are calculated assuming a "focusing frequency" f_0, representative of the signal frequency [*Hung and Kaveh*, 1988]. Since we use a relatively wide band of 1–4 Hz, the variations in tremor frequency induce

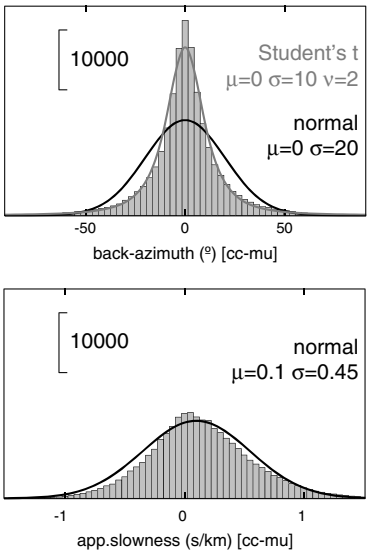

Figure 13. Histograms of the differences of back azimuth and apparent slowness estimates provided by the ZLCC and MUSIC methods. Bold lines represent probability distributions with the parameters given: mean (μ) and standard deviation (σ) for the normal distribution and location (μ), scale (σ), and degrees of freedom (ν) for the Student's *t* distribution.

variations in apparent slowness. The apparent slowness estimate S_{MU} for a signal of frequency f is related to the real apparent slowness S as follows:

$$S_{MU} = \frac{f}{f_0} S \tag{1}$$

This implies that MUSIC may underestimate/overestimate the apparent slowness when the frequency of the signal is below/above the focusing frequency. In our case the focusing frequency is 2.54 Hz; thus, the apparent slowness estimates might range from 40% (for 1 Hz) to 160% (for 4 Hz) of the real values. This effect is irrelevant for LP events because of their broadband frequency content, but it might be significant for harmonic tremors. The comparison with the ZLCC estimates allows us to detect the occurrence of this effect.

Notice that the apparent slowness shown along the paper are the raw estimates obtained with MUSIC and ZLCC. MUSIC results for harmonic tremors have not been corrected by the effect of the difference between the fundamental frequency and the focusing frequency, described above. This correction might vary slightly the actual values of apparent slowness, which would be increased for low-frequency signals and decreased for high-frequency signals. Most part of the harmonic tremors have fundamental frequencies in the 2–2.5 Hz range, which would explain the slight difference between the ZLCC and MUSIC estimates. In any case, the differences are not large enough to modify our interpretation of the results.

On the other hand, the ZLCC method is not designed for multiple wavefield components. Yet it is somewhat able to detect their presence when the apparent slowness vectors are different enough. For example, when two wave components propagate with different azimuths, ZLCC provides solutions that jump from one to the other (Figures 12a and 12c). The method is less sensitive to changes in apparent slowness, and when waves with different apparent slowness are involved, it yields a single solution between the apparent slowness provided by MUSIC (Figures 12b and 12c). In general, all these solutions have low MACC values.

Figure 14 shows a detailed view of what the array sees during one of these intervals with multiple wavefield components. The distributions of average cross correlation and MUSIC power correspond to a period at the center of Figure 12a. Initially, there is a single peak with back azimuth of ~50°N and apparent slowness of ~2 s/km. Later, we notice the appearance of a secondary peak with back azimuth of ~100°N and similar apparent slowness that eventually becomes dominant. MUSIC is able to identify both signals; however, ZLCC provides either one or the other.

5.2. LP Events

Our results indicate that LP events display three phases with similar propagation azimuths and increasing apparent slowness. The back azimuths of these three phases are 80±10°, which coincide with the array-crater direction of 85°N. On the contrary, the three phases have different behaviors in terms of apparent slowness. The first phase is a faint arrival characterized by a small apparent slowness of 0.4 s/km and a linear polarization in the incidence plane, implying near-vertical incidence of body waves, i.e., *P* waves. There is a second phase with intermediate apparent slowness of 1.1 s/km, followed by a third phase with high apparent slowness of 1.7 s/km. The large apparent slowness and the complex particle motions point to the presence of surface waves. Both late phases display large amplitudes, specially the third one. The delays of the second and third phases relative to the first are about 1.5 and 4.4 s.

Our interpretation of these apparent slowness vector results in terms of source position and characteristics is limited basically by the use of a single seismic array and our poor knowledge of the seismic velocity structure. Single-array source locations rely on a proper representation of wave propagation through the medium [*Goldstein and Chouet*, 1994; *Almendros et al.*, 1999; *Ibáñez et al.*, 2003], and thus, they are severely

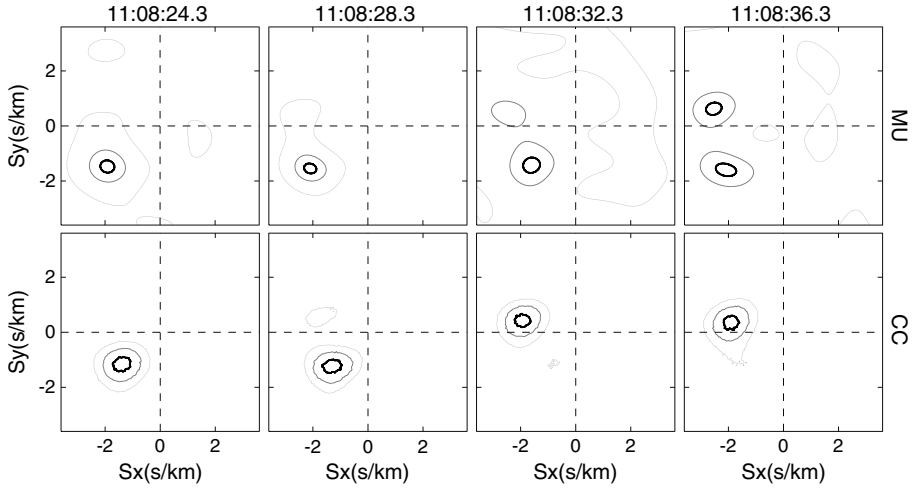

Figure 14. Distributions of (top row) MUSIC power and (bottom row) average cross correlation in the apparent slowness vector plane during a change in the dominant component of the harmonic tremor wavefield at about 11:08:30 on 23 February 2004.

affected by uncertainties in the velocity model. On the other hand, multiple arrays allow for quantitative estimates of source locations [*Almendros et al.*, 2001a, 2001b; *Metaxian et al.*, 2002; *La Rocca et al.*, 2004; *Saccorotti et al.*, 2004; *Di Lieto et al.*, 2007; *Ryberg et al.*, 2010; *Inza et al.*, 2014].

Although we cannot determine precisely the source location, we can use our apparent slowness and back azimuth results to constrain the source region of LP events. Taking into account the coincidence of the LP back azimuths with the direction to the volcano summit, we assume that LP epicenters are likely located in the crater area. For a fixed epicentral distance, the apparent slowness of a body wave generally decreases with increasing source depth. Thus, the small apparent slowness of the *P* wave might suggest that LP events originate in a relatively deep source. Nevertheless, the apparent slowness of a seismic phase depends not only on the source depth but on the velocity structure of the medium as well. An adequate interpretation of apparent slowness in terms of source depth requires some knowledge of the velocity structure.

The velocity structure of Arenal volcano has been investigated by *Mora et al.* [2006]. They performed refraction surveys on the east and west flanks of the volcano and applied the spatial autocorrelation (SPAC) method to calculate velocity models under two small-aperture, semicircular arrays. One of these models coincides with our array site. The model contains very slow and very thin shallow layers that may affect critically seismic wave propagation (e.g., *Vp* is 300 m/s for the first 3 m). In any case, *Mora et al.* [2006] shows that the structure of Arenal is complex and varies in length scales smaller than 100 m. For low-frequency signals, the involved wavelengths are larger than the layer thicknesses, and thus, we cannot rely on ray theory to image the seismic wave behavior. Full-wavefield numerical simulations are required to understand wave propagation.

Metaxian et al. [2009] performed wave propagation simulations in a 3-D model of Arenal volcano including topography. They combined the velocity models of *Mora et al.* [2006] to define a general model that could be useful for low-frequency signals. This model has two layers with thicknesses of 100 and 250 m and *P* wave velocities of 2.0 and 2.5 km/s, over a half-space with *P* wave velocity of 3.5 km/s. Layer interfaces follow the topography. *Metaxian et al.* [2009] used a 3-D elastic lattice approach [*O'Brien and Bean*, 2004] to generate the seismic wavefield recorded by a set of 35 nine-receiver seismic antennas distributed in a grid around the volcano at distances up to 8 km. They estimated the apparent slowness vectors at these arrays using the method of *Metaxian et al.* [2002] for different source locations and mechanisms. Their results show that for a source located at a depth of about 500 m beneath the crater, the synthetic array closest to our array site measures back azimuths pointing to the crater, with a slight northward deviation related to topography. Apparent velocities measured for the synthetic wavefields are 2–3 km/s. These velocity values correspond to apparent slowness of 0.3–0.5 s/km, which coincide with the range we observe for the *P* waves. Using these results, we conclude that our apparent slowness estimates could be fully compatible with a source located at shallow depths (<500 m) below the summit.

Moreover, our results show that the second and specially the third LP phases have large apparent slowness, which suggests that they are most likely composed of surface waves. And, remarkably enough, they have also large amplitudes, indicating a significant contribution of surface waves to the LP event waveform. A deep source is not an efficient generator of surface waves. The dominant presence of surface waves in the LP events also supports their origin in a shallow source.

This conclusion agrees with most studies of LP events at Arenal volcano that hint to a shallow source located a few hundred meters below the summit craters [*Alvarado et al.*, 1997; *Hagerty et al.*, 2000; *Lesage et al.*, 2006; *Davi et al.*, 2010; *Valade et al.*, 2012]. Explosion quakes with acoustic phases are assumed to be very shallow, while LP events are slightly deeper [*Valade et al.*, 2012]. These conclusions are supported by considerations about the characteristics of the acoustic source [*Benoit and McNutt*, 1997; *Garces et al.*, 1998] and are consistent with most of the observations. For example, *Hagerty et al.* [2000] analyzed LP events recorded between 1995 and 1997 with a five-station seismic network and a linear array deployed at Arenal volcano. They identified three phases in the LP onset and were able to measure apparent velocities at the array. These phases propagated at about 3.0, 1.3, and 0.6 km/s, corresponding to apparent slowness of 0.3, 0.8, and 1.7 s/km that are compatible with our results. *Hagerty et al.* [2000] interpreted the emergent, low-amplitude phase as a *P* wave; the second, more energetic phase as *S* wave energy; and the third phase as surface waves traveling within the shallow unconsolidated layers of the volcano edifice. They reported a delay of 1.0 ± 0.3 s between the *P* and *S* phases. Furthermore, they used *P* wave arrival times and a homogeneous half-space with *P* wave velocity of 2.5 km/s to locate the LP sources. The results point to a source region located at a depth of ~2 km below the summit. However, further analyses and comparisons of the relative timing between seismic and acoustic waveforms of explosion quakes led them to suggest that the seismic source should be much shallower. *Metaxian et al.* [2002] deployed four seismic arrays around Arenal volcano in 1997, at distances from the summit between 2 and 3.8 km. They performed a geometrical joint location [*Almendros et al.*, 2001a] using back azimuth estimates of LP events and explosion quakes. Their results show that the epicenters are located in the crater area, within 400 m of the active crater. Finally, *Davi et al.* [2010] used data from a nine-station broadband network deployed in 2005 to perform a moment tensor inversion of an LP event. They searched for the most likely point source location and mechanism and concluded that the LP waveform is adequately represented by an isotropic explosion located at very shallow depths below the crater (~200 m).

The timing of the LP phases following the *P* wave is another constraint that must be met. In this case, the simulations of *Metaxian et al.* [2009] do not coincide with the observations. If we interpret our second LP phase as *S* wave energy [*Hagerty et al.*, 2000], then the observed delay between the *P* and *S* phases is ~1.5 s. This value triplicates the predicted delay of ~0.5 s for a source at 500 m depth below the craters. The situation is even worst for the surface waves reaching the array 4.4 s after the *P* wave. These values seem too large for a source located at an epicentral distance of 2 km. It is likely that the shallow, unconsolidated layers of the volcano edifice play an important role in the large delays observed. A more detailed velocity model of Arenal volcano would be required to reproduce the observed delays of the seismic phases.

5.3. Volcanic Tremor

The analysis of the volcanic tremor wavefield reveals that spasmodic tremor is an incoherent signal that cannot be simply fitted by plane wavefronts. On the contrary, harmonic tremor is highly coherent. Apparent slowness values range mostly between 1 and 2 s/km. Propagation azimuths are variable, covering a broad span up to $\pm 40°$ from the crater-array direction. There is a significant dispersion in the solutions corresponding to different volcanic tremor episodes, especially in back azimuth. Changes in back azimuth are also observed within single-tremor episodes.

The large apparent slowness and the complex particle motions suggest that volcanic tremor at Arenal is composed of a mixture of surface waves. This coincides with observations of the seismic wavefield at other volcanic areas [e.g., *Almendros et al.*, 1997; *Metaxian et al.*, 1997; *Chouet et al.*, 1998; *Konstantinou and Schlindwein*, 2002; *Saccorotti et al.*, 2001, 2004; *Ibáñez et al.*, 2008]. The range of apparent slowness of 1–2 s/km corresponds to apparent velocities between 0.5 and 1.0 km/s. *Mora et al.* [2006] analyzed data from a seismic array deployed at the same location we have used in this work and found a dispersion curve for Rayleigh waves with phase velocities of 0.95, 0.76, and 0.56 km/s for 1, 2, and 4 Hz, respectively. These values fall within the apparent velocity range determined by our array, which indicates that surface waves dominate the tremor wavefield.

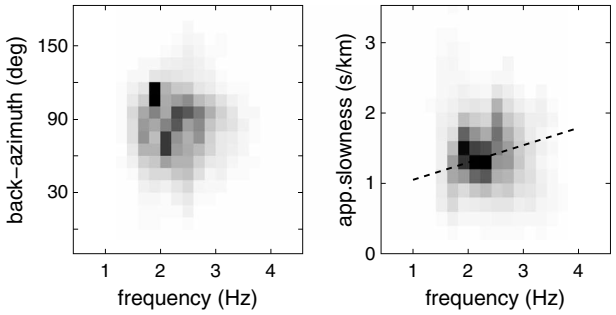

Figure 15. Distributions (2-D histograms) of back azimuth and apparent slowness versus fundamental frequency for harmonic tremors. We use ~38,500 simultaneous estimates of apparent slowness vectors and tremor frequencies obtained along the data set. The color scale ranges from 0 (white) to 1700 (black). The dashed line indicates the approximate position of the dispersion curve determined by *Mora et al.* [2006].

In spite of this coincidence, we have not found evidences of surface wave dispersion. In principle, harmonic tremors with different fundamental frequencies would sample the medium to different depths, and thus, they should propagate with phase velocities that decrease with increasing tremor frequency. We have used the semiautomated method of *Lesage* [2009] to measure the fundamental frequency of harmonic tremors along the data set. We assign the apparent slowness vectors corresponding to the main peak of the MUSIC spectra to these fundamental frequencies. The resulting distributions (Figure 15) indicate that the range of apparent slowness coincides with the values obtained by *Mora et al.* [2006]. It is also clear that the apparent slowness of harmonic tremor shows only a very loose correlation with frequency, even if we correct the MUSIC estimates of apparent slowness for the effect of the difference between the signal frequency and the focusing frequency. The scatter of solutions is too large, which might indicate the occurrence of other processes masking the effect of surface wave dispersion.

The location of the volcanic tremor source is a difficult task that has to be approached with unconventional techniques such as array analyses [*Metaxian et al.*, 1997; *Almendros et al.*, 1999, 2001a, 2001b; *La Rocca et al.*, 2004], seismic amplitude distributions [*Battaglia and Aki*, 2003; *Battaglia et al.*, 2005; *Patane et al.*, 2008; *Haney*, 2010], moment tensor inversions [*Davi et al.*, 2012], and time reversal imaging [*Lokmer et al.*, 2009]. Attempts to determine the position of the volcanic tremor source at Arenal volcano suggest that it is located at shallow depths beneath the craters, basically coinciding with the source of the LP events. For example, *Metaxian et al.* [2002] used a probabilistic source location approach based on back azimuth estimates obtained with multiple seismic arrays deployed around the volcano. They analyzed a set of 45 records of volcanic tremor and found that the most likely epicenter locations clustered within 600 m of the summit craters. *Davi et al.* [2012] used an approach based on moment tensor inversions of the tremor waveforms. They found that the most likely source mechanism is a subhorizontal crack located within a few hundred meters of the active crater. Source depth is estimated to be just ~100 m.

Apart from these direct estimates, investigations of the source process of harmonic tremor yield pressure ranges compatible with a shallow source under the crater [*Benoit and McNutt*, 1997; *Garces et al.*, 1998; *Hagerty et al.*, 2000; *Lesage et al.*, 2006].

These results raise an interesting question. If the source is indeed located in a shallow volume beneath the volcano summit, then why do we retrieve such a wide span of tremor back azimuths? We observe back azimuths from 40 to 120°N for different tremor episodes. Moreover, we find temporal changes during apparently stable harmonic tremors, including both rapid jumps and smooth variations in scales of tens of seconds. These results seem to suggest the presence of an extended source region. The activation of different parts of this source would produce tremors with different propagation azimuths. Jumps in the propagation parameters would be produced by the alternate activation of two different sections of the extended source, situated at different positions within the volcano. Gradual variations would respond to the horizontal displacement of the active section of the conduits where tremors are generated. However, the magnitudes of the variations observed in the propagation azimuths amount to many tens of degrees. This result seems to imply an unrealistically large source extent of the order of the source-array distance, which is incompatible with a shallow tremor source at the volcano summit.

Nevertheless, we must consider that seismic wavefields propagating in a heterogeneous medium may be subject to important distortions. These distortions are particularly noticeable at volcanoes, generally characterized by heterogeneous velocity structures and rough topographies. Wave propagation effects have been investigated at several volcanoes, for example, using active source experiments [*La Rocca et al.*, 2001; *Nisii*

et al., 2007; *García-Yeguas et al.*, 2011] and numerical simulations [*Almendros et al.*, 2001a; *Bean et al.*, 2008; *O'Brien and Bean*, 2009; *Metaxian et al.*, 2009; *Kumagai et al.*, 2011]. These results indicate that propagation azimuths may deviate up to several tens of degrees from the source-receiver direction, even in short distances. Thus, a back azimuth estimate is not directly interpretable in a geometrical sense as pointing straight back to the source. In our case, it is likely that the heterogeneity of the velocity structure of Arenal volcano and its rough topography produce important distortions in the seismic wavefield. In particular, tremor wavefields would be most sensitive to propagation effects, since they are mainly composed of surface waves that propagate within the shallowest, most heterogeneous layers of the volcano.

The image that emerges is that of a complex source region with small-scale heterogeneities generating a variable seismic radiation pattern and complex propagation effects producing lateral deviations of the seismic wave paths. Given that in general the medium does not change significantly its properties in short time scales, a perfectly stationary source would produce waves propagating across the array from a definite direction. It might not coincide with the source-array direction due to path effects, but it would be constant throughout the data set. Thus, the processes ultimately responsible for the azimuth variability of volcanic tremor must occur within the source region. This region located at shallow depths below the volcano summit is the locus of highly dynamic energy exchanges between the magma mix, the solid rock, and the atmosphere. It is subject to rapidly changing physical conditions that may affect the location, depth, and even the mechanism of the tremor-generating processes.

Evidences of changing conditions in the source region are described by *Valade et al.* [2012]. They compared seismic data and Doppler radar measurements of pyroclastic emissions obtained at Arenal volcano in 2005. These data allowed them to investigate the relationship between gas and tephra emissions. They found a very poor correlation between the occurrence and characteristics of seismic activity and tephra emissions imaged by radar. To explain this striking observation, *Valade et al.* [2012] proposed a conceptual model where the shallow system properties (plug thickness, rheology, fracturing, and permeability) are utterly variable, thus yielding nonrepeatable conditions that may account for the disconnection between radar and seismic signals.

The volcano edifice limits the horizontal extent of a shallow source region to a radius of a few hundred meters. This size could be enough to explain our observations, provided that important path effects take place. Small variations in the source position, depth, or mechanism may produce large differences in the path followed by the seismic waves. For example, we could imagine a low-velocity zone between the source and the array, producing a "lens effect." This geometry was discussed by *García-Yeguas et al.* [2011] in their interpretation of the apparent slowness vectors observed during an active source experiment at Deception Island volcano. Waves originating in the north part of the source region would be deflected southward and arrive at the array site with a counterclockwise rotation of the apparent slowness vectors, as compared to the source-array direction. Similarly, waves originating in the south of the source region would be deflected northward (clockwise rotation of the apparent slowness vector). Another structure that could be considered is the interface between the pre-1968 and post-1968 edifices at Arenal volcano. *Lindquist et al.* [2007] analyzed the bias in the apparent slowness vector estimates produced by a dipping Moho discontinuity beneath a medium-aperture seismic array located in Alaska. They concluded that this discontinuity produced deviations in azimuth that depend on the source position relative to the dipping layer. For a flat surface, the magnitude of the deviations as a function of source back azimuth follows a cosine function. Maximum deviations of $\sim 10^\circ$ occur for sources located in directions that parallel the strike of the dipping interface. Although the scales are different, and the interface between the pre-1968 and post-1968 edifices is not flat, these results could indicate that the old cone discontinuity might bear an important weight in the observed spreading of the tremor back azimuth estimates.

We conclude that propagation effects due to the topography and heterogeneous velocity structure could be able to amplify the small changes that occur within the source volume, thus yielding the wide span of back azimuths observed. In this interpretation, the variability of the tremor back azimuths reflects the coupled effect of changing conditions at the source and heterogeneity of the velocity structure.

5.4. Simultaneous Harmonic Tremor Sources

On top of the complexity of the volcanic tremor wavefields described above, we have found that in several periods our results hint to the presence of multiple, simultaneous harmonic tremors in the seismic wavefield of Arenal volcano. Evidences are: (1) the visual identification in the spectrograms of multiple, simultaneous

groups of harmonics that evolve independently, (2) the development of complex spatial amplitude patterns related to wave interference, and (3) the appearance of multiple apparent slowness vectors in the MUSIC solutions.

The first indication of simultaneous tremor sources is the observation of multiple sets of harmonics in the spectrogram of harmonic tremor, which evolve independently (e.g., Figure 4). Simultaneous sets of harmonics at Arenal volcano have been described by *Lesage et al.* [2006]. They analyzed the spectral behavior of harmonic tremors and concluded that at some periods two sources were active within the volcano. *Lesage et al.* [2006] also reports the simultaneous observation of gas emissions from two active vents, which supports their interpretation. Reports of harmonic tremors with multiple sets of harmonics are indeed very rare in the literature, which emphasizes the interest of the present analysis. Apart from Arenal, we could find just one description of multiple sets of harmonics in the seismic signals associated to large icebergs [*Aster et al.*, 2004]. However, this kind of behavior is quite common in our data set (Figure 5).

The second indication comes from the analysis of the seismic amplitudes at the array stations. *Almendros et al.* [2012] used our same data set to describe the anomalous behavior of the harmonic tremor amplitudes observed at the seismic array. They found strong variations among the amplitudes of sustained harmonic tremors recorded at the different array stations. The resulting amplitude patterns were geometrically complex, they were stable over periods of a few tens of seconds but changed with time on longer time scales, and they were related solely to harmonic tremors and disappeared when any other type of seismicity dominated the wavefield. *Almendros et al.* [2012] interpreted these complex amplitude patterns as a result of wave interference among different signals composing the harmonic tremor wavefield. Thus, we propose that the complexity of the spatial distribution of tremor amplitudes might indicate the simultaneous activation of multiple tremor sources.

Finally, the third indication comes from the results of our array analysis of the tremor wavefield. The application of the MUSIC algorithm to harmonic tremors sometimes produces two high-PMUP estimates indicating the presence of two significant wave components with different propagation properties (Figure 12). The differences may occur in apparent slowness, back azimuth, or both. Harmonic tremor wavefields are generally characterized by apparent slowness in the range 1–2 s/km. Whenever MUSIC provides two solutions with different apparent slowness, one of the components has an apparent slowness of 0.5–1.5 s/km while the other has a large apparent slowness of 2–3 s/km (Figure 12). These slownesses are of the same order as the slowness of sound in the air and suggests a link with the propagation of acoustic waves in the atmosphere. In other instances there are large differences in the back azimuths, and none of them point directly to the crater. This observation is difficult to reconcile with a single-tremor source located at the volcano summit. However, as discussed above, it could be explained by the combination of a complex source region with multiple active sections and strong propagation effects due to the topography and heterogeneous shallow structure of the volcanic medium.

We have reviewed the occurrence of these three wavefield characteristics in our data set to investigate the presence of multiple, simultaneous tremor sources. We presume that these effect should be somehow related, since all of them are evidences of a dual tremor source. Figure 16 shows the spectrograms, average amplitudes, and back azimuth estimates of harmonic tremors corresponding to different periods. Figures 16a–16d are samples of harmonic tremor whose spectrograms show a single set of harmonics. On the contrary, Figures 16e and 16f display spectrograms where two different sets of harmonics evolving independently can be clearly identified, thus suggesting a double tremor source. Figures 16a–16c show harmonic tremors with strong differences of seismic amplitude among array stations, originated by the interference of two wavefield components. On the contrary, Figures 16d–16f display harmonic tremors with similar amplitudes at all stations. Average amplitudes are measured using the RMS of the seismic waveform in 10 s long windows [*Almendros et al.*, 2012]. Figures 16b, 16d, and 16f illustrate the clear detection of two wavefield components with different back azimuths. On the contrary, Figures 16a and 16e correspond to a wavefield with a single, dominant wavefield component.

From these plots, we find that there is no clear relationship between the presence of multiple sets of harmonics, a complex amplitude pattern, and MUSIC detection of two wavefield components. In fact, these effects can appear alone while the other two are absent, as revealed by Figures 16a (amplitude pattern), 16d (dual MUSIC solutions), and 16e (two sets of harmonics). Figure 16b shows both amplitude differences and two MUSIC solutions. Figure 16f shows both a double set of harmonics in the spectrogram and two MUSIC

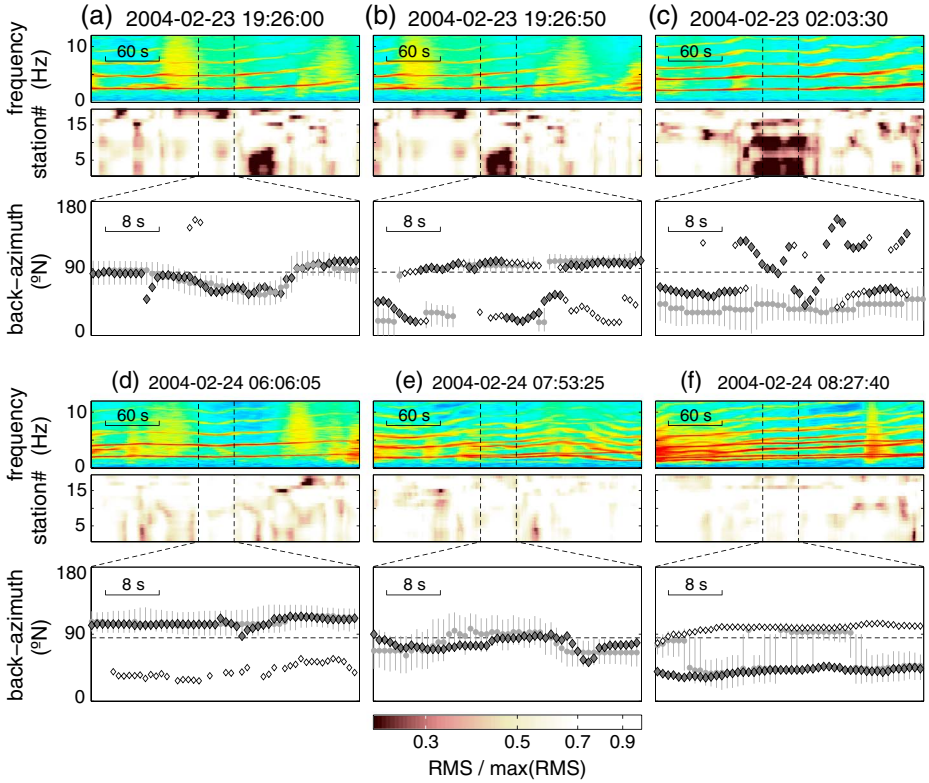

Figure 16. (a–f) Comparison among evidences of multiple harmonic tremor sources. We show, from top to bottom, the spectrogram, color-coded average amplitude versus time at each array station, and back azimuth estimates. The time label indicates the start of the back azimuth time window. Window lengths are 5 min for the top and middle rows and 40 s for the bottom row.

solutions. The only combination that seems incompatible is the simultaneous occurrence of two sets of harmonics and a complex amplitude pattern at the array.

The complex spatial amplitude patterns usually occur during clean, relatively stable sections of harmonic tremor, as already noticed by *Almendros et al.* [2012]. They do not occur when multiple sets of harmonics crisscross in the spectrogram. *Almendros et al.* [2012] proposed that the amplitude patterns at the array are produced by interference of two wavefield components. If this is the case, the presence of these two interfering signals is not evident from the spectrograms. The reason we cannot see them could be that the two wave components have different apparent slowness vectors but similar frequencies. *Almendros et al.* [2012] showed that the positions of the crests of the interference pattern of two plane waves are related to the difference of frequency between them. When the waves have the same frequency, the pattern is stationary. When the waves have different frequencies, the patterns evolve with time. Our method to identify the occurrence of complex amplitude patterns is based on the measure of the average wave amplitudes in 10 s long windows [*Almendros et al.*, 2012]. Thus, we may fail to detect them if the amplitude ratios vary on time scales much shorter than 10 s. That is, we cannot detect a clear interference pattern unless the difference of frequencies is smaller than 0.1 Hz.

In summary, all these observations indicate that harmonic tremors are highly complex signals. They result from time-varying single or double sources. The precise wave propagation paths in the heterogeneous medium depend critically on the location and characteristics of the source. The combination of strong source and path effects produces the variety of features revealed by the spectral, array, and amplitude analyses.

5.5. Relationship Between LP Events and Tremor

At many volcanoes around the world, LP events and volcanic tremor are intimately linked. They usually share similar spectral characteristics, source locations, wave propagation parameters, etc [*Almendros et al.*, 1997;

Chouet et al., 1997; *Arciniega Ceballos et al.*, 2000; *Neuberg et al.*, 2000; *Almendros et al.*, 2001b; *Saccorotti et al.*, 2001; *Metaxian et al.*, 2002]. These observations have led to the widely assumed notion that volcanic tremor is the consequence of the sustained repetition of the LP generation mechanisms. In other words, volcanic tremor is viewed as a superposition of closely spaced LP events [*Chouet*, 1988, 1996, 2003; *Almendros et al.*, 1997; *Neuberg et al.*, 2000; *Arciniega Ceballos et al.*, 2003; *Kawakatsu and Yamamoto*, 2007].

On the contrary, at a few other volcanoes there seems to be a disconnection between LP events and tremor. For example LP events and tremor during the 2004–2005 effusive episode of Etna volcano displayed different spectral characteristics and source locations [*Saccorotti et al.*, 2007; *Cannata et al.*, 2009]. *McNutt and Nishimura* [2008] compared the characteristics of explosion quakes and eruption tremor recorded during 24 eruptions at 18 volcanoes. Several parameters are different for each type of signal, e.g., the relationships between seismic magnitude and vent radius. Explosion quakes have larger magnitude than tremor for similar vent sizes. These differences are attributed to the fact that explosions need a high pressure to break the closing cap, while tremor is related to small-pressure fluctuations in an open system.

At Arenal volcano, LP events and tremor have different spectral features, although they apparently share the same source region [*Metaxian et al.*, 2002; *Davi et al.*, 2010, 2012]. In reality, LP events at Arenal are small explosion quakes. Their mechanisms are related to the explosive emissions that take place beneath the craters, while tremors are related to steady degassing. LPs and tremor are occasionally associated [e.g., *Hagerty et al.*, 2000; *Lesage et al.*, 2006]. Harmonic tremor may develop in the coda of the LP events (Figure 3a). This suggests a cause-and-effect relationship, that is, tremor occurs as a consequence of the explosion quake. However, these events may also occur independently, indicating that this relationship is not systematic.

Our results indicate that LP and tremor wavefields have different propagation characteristics. We underline two differences between our apparent slowness vector estimates for LP events and tremor. First of all, they are stable for LP events and utterly variable for tremor. The stability of the apparent slowness vectors of LP events suggests that the source locations and mechanisms are consistently the same from event to event throughout our entire data set. Therefore, LP events originate in a single, precise section of the plumbing system below the craters. On the contrary, tremor directions are highly variable. We attribute this variability to the coupled effect of the changing conditions in the source region, which produces variable radiation patterns, and path effects due to topography and heterogeneous shallow velocity structure. The variability in the apparent slowness vectors of harmonic tremors and the evidences of multiple sources point to an extended, complex, and unstable source region where the precise location and mechanism of a tremor source may change rapidly.

The second difference is that LP events propagate with back azimuths pointing to the volcano summit, while harmonic tremors display a wide range of back azimuths. Harmonic tremor wavefields seem to be deflected up to tens of degrees, while LP events are scarcely affected by path effects. This may be due in part to the difference in wave types. The early phases of LP events are body waves, while tremor is composed of surface waves. Body waves penetrate to some depth in the medium, while surface waves develop in the unconsolidated shallow layers. The velocity structure probably homogenizes with depth, due, for example, to compaction [*Alvarado et al.*, 2010]. Thus, we expect smaller lateral deflections for body waves than for surface waves. This observation is confirmed by the numerical simulations of wave propagation performed by *Metaxian et al.* [2009]. In these simulations, the source direction is generally well retrieved by synthetic arrays, even at large distances from the volcano. However, we have to keep in mind that *Metaxian et al.* [2009] used a simplified model of Arenal volcano, where the shallow, low-velocity layers and the heterogeneous 3-D structure are not completely reproduced. It may be a realistic model for body waves but not so much for surface waves.

In any case, the difference of wave type does not explain why the late phases of LP events, composed of surface waves, have apparent slowness vectors pointing to the crater area (just as the *P* waves). There is some scatter in back azimuth for large apparent slowness (Figure 7), specially toward the north. This can be also seen in Figure 6, where the back azimuth estimates corresponding to the late LP phases are systematically smaller (i.e., northward) than the array-crater direction. These slight northward deviations might be related to topographic effects, as hinted by the numerical simulations of *Metaxian et al.* [2009] for a synthetic array located near our array site. But in spite of this small deflections, it is clear that propagation effects do not influence the surface waves of LP events in the same way that they alter the surface waves composing the

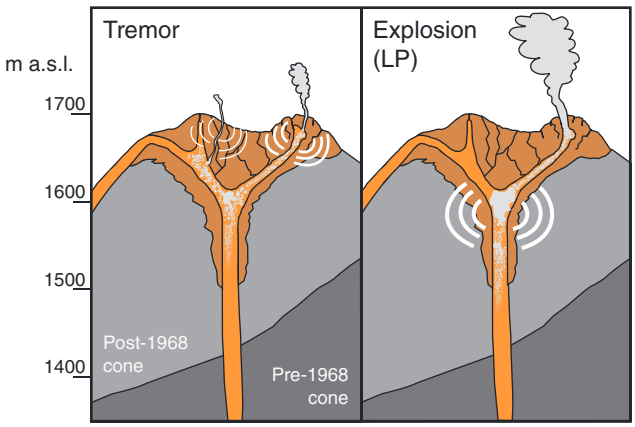

Figure 17. Sketch of the plumbing system under the C crater of Arenal volcano and the mechanism generating (left) volcanic tremor and (right) explosion quakes and LP events. Gray shapes within the volcanic conduits represent gas bubbles and pockets. White lines mark the conduit sections where the main seismic radiation must take place to account for the differences observed between the wavefields of volcanic tremor and LP events. The thicknesses of these lines indicate the intensity of seismic radiation, which is generally largest for LP events.

tremor wavefields. What property could explain this difference between surface waves from LPs and tremor? Surface waves of LP events are short-lived and relatively broadband, while tremor is a long-lasting signal of harmonic character. The differences in bandwidth could affect wave propagation, for example, through wave dispersion. Nevertheless, since the dominant frequencies for both signals are about the same, the radically different behaviors in terms of propagation azimuth are difficult to explain.

Source depth may be another factor to take into account. Tremor is generated near the surface; thus, seismic waves travel within the shallow, unconsolidated, low-velocity layers of the volcano. LP events are deeper, and thus, surface waves are generated closer to the array. In any case, the behavior of surface waves from LP events and tremor at Arenal volcano remains still an open question.

5.6. Source Model

Several models have been proposed to account for the generation of volcanic tremor at Arenal volcano, such as the resonance of a fluid-filled pipe [*Benoit and McNutt*, 1997; *Garces et al.*, 1998], the nonlinear excitation of an irregular channel by fluid flow [*Hagerty et al.*, 2000], or the clarinet model based on the regular repetition of fast degassing events modulated by the resonance of the conduit [*Lesage et al.*, 2006]. More recently, *Valade et al.* [2012] propose a model for both LP events and tremor. The scenario includes a gas-rich magma under a solid lava cap. If gas release through fractures in the cap is intermittent, repetitive pressure pulses generate volcanic tremors. If gas release is sudden, flow-induced vibrations generate explosion quakes. Thus, an LP event is a consequence of the sudden release of large quantities of gas when the inner pressure overcomes the cap strength, while volcanic tremor implies continuous degassing, small-pressure fluctuations, and rapid openings and closures of cracks. In this model, the physical processes for tremor and LP events are thought to be similar and to occur in the same source region. Their difference lays in the strength and temporal behavior of the excitation mechanism. The results of the present paper seem to be inconsistent with this model, because they demonstrate that the characteristics of the seismic wavefields generated by LP events and tremor are substantially different, as illustrated by Figures 7 and 10.

In order to take the differences between LP event and tremor wavefields into account, the model proposed by *Valade et al.* [2012] requires further precisions, which are sketched in Figure 17. Harmonic tremor is produced by repetitive gas pulses through fractures in the plug that are stabilized by conduit resonance. Using numerical modeling of seismic waves in a conduit, *Jousset et al.* [2003] demonstrated that seismic energy is mainly radiated at the top end of the conduit and further propagates as surface waves. The seismic source of harmonic tremor, which results from the combination of fracture oscillations and coupled conduit resonance, is thus located in the very shallow and heterogeneous part of the crater (Figure 17 (left)). It produces a wavefield mainly composed of surface waves and is quite sensitive to small variations in the velocity structure. On the other hand, although the emission probably occurs in the same vents for tremor and LP events, the volume and flux of gas and solid particles involved are much larger for the latter type of event. This material is either accumulated below the plug or produced by fragmentation in the upper conduit triggered by rapid pressure decrease. In this case, the seismic radiation mostly occurs at larger depth in the conduit, say a few hundreds of meters (Figure 17 (right)). Thus, the initial part of the wavefield is composed of body waves. The interaction of the body waves with the free surface produces surface waves. However, this process occurs at some distance from the source and thus at a closer distance to the array than the source of

tremor. The surface waves that compose the later part of the LPs are thus less affected by the structural heterogeneities. This explains why their slowness vectors point to the crater. This interpretation is also consistent with results of moment tensor inversion which indicate that the sources of LP events are slightly deeper than those of volcanic tremors [*Davi et al.*, 2010, 2012].

6. Conclusions

We carried out a detailed analysis of the seismic wavefield produced by tremor and LP events in the complex and heterogeneous structure of Arenal volcano. The processing of data recorded by a single small-aperture spiral-shaped array with high-quality response allowed good resolution in the estimation of the apparent slowness vectors. We used two array processing techniques, the zero-lag cross correlation and the multiple signal classification method, with similar parameters. To our knowledge, it is the first time that these two methods have been systematically compared. Both methods yield consistent results, especially in azimuth. Apparent slownesses show slight discrepancies that can be attributed to a methodological difference.

Our results indicate that LP events are characterized by stable back azimuths that point toward the crater with small fluctuations of $\pm 10°$. Their onset include three phases with different slowness and polarizations which indicate the arrival of *P* and surface waves. Harmonic and spasmodic tremors present more complex features. Their apparent slownesses are around 1–2 s/km, and their propagation azimuth varies in an interval as wide as $\pm 40°$ around the crater-array direction. These parameters are generally stable but may vary either smoothly or sharply, indicating substantial changes in the source region. Moreover, we document evidences of multiple simultaneous tremor sources, for example, independent sets of harmonics in the spectrograms, complex spatial amplitude patterns related to wave interference, and multiple solutions in the MUSIC method. No relationship has been found among these evidences of multiple sources. We conclude that the complexity of volcanic tremor wavefields at Arenal volcano must result from a combination of source and path effects. Tremors must originate in a highly complex region subject to rapid changes of physical conditions and able to produce simultaneous radiation from different seismic sources. This source variability, coupled with important path effects related to the topography and shallow velocity structure, may be held responsible for the large spread in the apparent slowness vector estimates.

The similarities and differences in the wavefield features of tremor and LP events provide insight into the origin and relationship of the two types of signal. Our interpretation is based on the source model proposed by *Valade et al.* [2012], with slight improvements. In this model, LP events and tremor are both generated in the shallow plumbing system below the craters. Degassing is controlled by the opening and closing of fractures in the rigid lava crust that covers the conduit. LP events are associated with the sudden release of large volumes of gas which produce radiation of seismic waves mostly from a depth of a few hundreds of meters below the crater. The location of this source is relatively stable. Body waves propagate mainly in a weakly heterogeneous medium, and their conversion in surface waves occurs at short distances from the array. Thus, both types of waves are not much perturbed by the structural heterogeneities and their back azimuths present only slight fluctuations.

Volcanic tremors are produced by pressure pulses due to intermittent gas flow through fractures in the solid cap. When the period of the pulses is stabilized by a feedback mechanism related to standing or traveling waves in the conduit, the spectrum includes many regularly spaced peaks [*Lesage et al.*, 2006]. The radiation of seismic waves mainly occurs at very shallow depth in a medium subject to rapid changes. At some moments, two sources of tremor can be active simultaneously. These sources produce dominant surface waves that travel from the crater to the array in heterogeneous layers. Hence, the coupled effect of source variability and propagation in a complex medium can explain the large scatter of observed apparent slowness and back azimuths which hides the dispersive properties of surface waves.

This study has demonstrated that LP events and tremor are characterized by distinct levels of complexity and different source depths. Thus, although both types of event originate in similar degassing processes at Arenal volcano, tremor cannot be considered exactly as the repetition of LP events. The results of the present work related to the complexity of seismic wavefields in volcanic structures and to the characteristics of the sources of seismovolcanic events could help interpreting observations on other volcanoes especially when seismic arrays are not available.

Acknowledgments
Seismograms used in this study were collected during a short experiment carried out by the Observatorio Sismológico y Vulcanológico de Arenal y Miravalles (OSIVAM-ICE) in February 2004. Data will be available after exploitation and can be obtained through request to Waldo Taylor Castillo (wtaylor@ice.go.cr). Some plots and analyses were made using MATLAB (www.mathworks.com). We are grateful to ICE for supporting the logistical work and the data acquisition. We are also grateful to the Arenal Conservation Area staff for the facilities provided during the field work. The financial support at different stages of the study was obtained from projects 113-A4-501, 113-A6-503, and 113-B4-082 from University of Costa Rica, the Ministry of Science and Technology (MICIT), and National Council for Scientific and Technological Research (CONICIT). Partial support was also provided by projects CTM2010-11740 and CGL2011-29499-C02-01 of the Spanish Ministry of Education. The comments and suggestions to the geological model and other features by Gerardo G. Soto and Guillermo E. Alvarado, from ICE, are kindly acknowledged. We also thank the JGR Associate Editor and two anonymous reviewers, whose thoughtful comments contributed to improve the manuscript.

References

Almendros, J., J. M. Ibáñez, G. Alguacil, E. Del Pezzo, and R. Ortiz (1997), Array tracking of the volcanic tremor source at Deception Island, Antarctica, *Geophys. Res. Lett.*, *24*(23), 3069–3072, doi:10.1029/97GL03096.

Almendros, J., J. M. Ibáñez, G. Alguacil, and E. Del Pezzo (1999), Array analysis using circular-wave-front geometry: An application to locate the nearby seismo-volcanic source, *Geophys. J. Int.*, *136*(1), 159–170, doi:10.1046/j.1365-246X.1999.00699.x.

Almendros, J., J. M. Ibáñez, G. Alguacil, J. Morales, E. Del Pezzo, M. La Rocca, R. Ortiz, V. Araña, and M. J. Blanco (2000), A double seismic antenna experiment at Teide volcano: Existence of local seismicity and lack of evidences of volcanic tremor, *J. Volcanol. Geotherm. Res.*, *103*(1–4), 439–462, doi:10.1016/S0377-0273(00)00236-5.

Almendros, J., B. Chouet, and P. Dawson (2001a), Spatial extent of a hydrothermal system at Kilauea Volcano, Hawaii, determined from array analyses of shallow long-period seismicity. 1. Method, *J. Geophys. Res.*, *106*(B7), 13,565–13,580, doi:10.1029/2001JB000310.

Almendros, J., B. Chouet, and P. Dawson (2001b), Spatial extent of a hydrothermal system at Kilauea Volcano, Hawaii, determined from array analyses of shallow long-period seismicity. 2. Results, *J. Geophys. Res.*, *106*(B7), 13,581–13,597, doi:10.1029/2001JB000309.

Almendros, J., J. M. Ibáñez, E. Carmona, and D. Zandomeneghi (2007), Array analyses of volcanic earthquakes and tremor recorded at Las Cañadas caldera (Tenerife Island, Spain) during the 2004 seismic activation of Teide volcano, *J. Volcanol. Geotherm. Res.*, *160*, 285–299, doi:10.1016/j.jvolgeores.2006.10.002.

Almendros, J., R. Abella, M. Mora, and P. Lesage (2012), Time-dependent spatial amplitude ratios of harmonic tremor at Arenal volcano, Costa Rica: Seismic wave interferences?, *Bull. Seismol. Soc. Am.*, *102*, 2378–2391, doi:10.1785/0120120066.

Alvarado, G., and I. Arroyo (2000), Los flujos piroclásticos del volcán Arenal (Costa Rica) entre 1975 y 2000: Origen, frecuencia, distribución y peligro asociado, *Boletín del Observatorio Sismológico y Vulcanológico de Arenal y Miravalles*, *12*, 39–53.

Alvarado, G., S. Carboni, M. Cordero, E. Aviles, and M. Valverde (2010), Stability of the cone and foundation of Arenal volcano, Costa Rica, in *Volcanic Rock Mechanics: Rock Mechanics and Geo-Engineering in Volcanic Environments*, edited by C. Olalla et al., pp. 135–150, Taylor and Francis Group, London.

Alvarado, G. E. (2011), *Los Volcanes de Costa Rica: Geología, Historia y Riqueza Natural*, 284 pp., EUNED, San Jose, Costa Rica.

Alvarado, G. E., and R. Barquero (1987), Las señales sísmicas del volcán Arenal (Costa Rica) y su relación con las fases eruptivas (1968–1986), *Cienc Tecnol.*, *11*, 15–35.

Alvarado, G. E., and G. J. Soto (2002), Pyroclastic flow generated by crater-wall collapse and outpouring of the lava pool of Arenal Volcano, Costa Rica, *Bull. Volcanol.*, *63*, 557–568, doi:10.1007/s00445-001-0179-9.

Alvarado, G. E., W. Taylor, M. Ohmberger, G. Soto, and L. Madrigal (1997), First observations of volcanic seismicity at Arenal volcano (Costa Rica) using a new three-component seismic digital network, *Boletín del Observatorio Sismológico y Vulcanológico de Arenal y Miravalles*, *15*, 11–45.

Alvarado, G. E., G. J. Soto, H.-U. Schmincke, L. L. Bolge, and M. Sumita (2006), The 1968 andesitic lateral blast eruption at Arenal volcano, Costa Rica, *J. Volcanol. Geotherm. Res.*, *157*(1–3), 9–33, doi:10.1016/j.jvolgeores.2006.03.035.

Arciniega Ceballos, A., C. Valdes Gonzalez, and P. Dawson (2000), Temporal and spectral characteristics of seismicity observed at Popocatepetl volcano, central Mexico, *J. Volcanol. Geotherm. Res.*, *102*(3–4), 207–216, doi:10.1016/S0377-0273(00)00188-8.

Arciniega Ceballos, A., B. Chouet, and P. Dawson (2003), Long-period events and tremor at Popocatepetl volcano (1994–2000) and their broadband characteristics, *Bull. Volcanol.*, *65*, 124–135, doi:10.1007/s00445-002-0248-8.

Aster, R., et al. (2004), Real-time data received from Mount Erebus Volcano, Antarctica, *Eos Trans. AGU*, *85*(10), 97–101, doi:10.1029/2004EO100001.

Barquero, R., G. E. Alvarado, and T. Matumoto (1992), Arenal volcano (Costa Rica) premonitory seismicity, in *Volcanic Seismology, IAVCEI Proceedings in Volcanology*, vol. 3, edited by R. Barquero, G. E. Alvarado, and T. Matumoto, pp. 84–96, Springer-Verlag, Berlin Heidelberg.

Battaglia, J., and K. Aki (2003), Location of seismic events and eruptive fissures on the Piton de la Fournaise volcano using seismic amplitudes, *J. Geophys. Res.*, *108*(B8), 2364, doi:10.1029/2002JB002193.

Battaglia, J., K. Aki, and V. Ferrazzini (2005), Location of tremor sources and estimation of lava output using tremor source amplitude on the Piton de la Fournaise volcano: 1. Location of tremor sources, *J. Volcanol. Geotherm. Res.*, *147*, 268–290, doi:10.1016/j.jvolgeores.2005.04.005.

Bean, C., I. Lokmer, and G. O'Brien (2008), Influence of near-surface volcanic structure on long-period seismic signals and on moment tensor inversions: Simulated examples from Mount Etna, *J. Geophys. Res.*, *113*(B8), B08308, doi:10.1029/2007JB005468.

Benoit, J. P., and S. R. McNutt (1997), New constraints on source processes of volcanic tremor at Arenal volcano, Costa Rica, using broadband seismic data, *Geophys. Res. Lett.*, *24*(4), 449–452, doi:10.1029/97GL00179.

Borgia, A., and S. R. Linneman (1980), On the mechanisms of lava flow emplacement and volcano growth: Arenal, Costa Rica, in *Lava Flows and Domes: Emplacement Mechanisms and Hazard Implications, IAVCEI Proceedings in Volcanology*, vol. 2, edited by J. H. Fink, pp. 208–243, Springer-Verlag, Berlin.

Borgia, A., C. Poore, M. J. Carr, W. G. Melson, and G. E. Alvarado (1988), Structural, stratigraphic, and petrographic aspects of the Arenal-Chato volcanic system, Costa Rica: Evolution of a young stratovolcanic province, *Bull. Volcanol.*, *50*, 86–105, doi:10.1007/BF01275171.

Cannata, A., M. Hellweg, G. Di Grazia, S. Ford, S. Alparone, S. Gresta, P. Montalto, and D. Patane (2009), Long period and very long period events at Mt. Etna volcano: Characteristics, variability and causality, and implications for their sources, *J. Volcanol. Geotherm. Res.*, *187*(3–4), 227–249, doi:10.1016/j.jvolgeores.2009.09.007.

Chouet, B. (1988), Resonance of a fluid-driven crack: Radiation properties and implications for the source of long-period events and harmonic tremor, *J. Geophys. Res.*, *93*(B5), 4375–4400, doi:10.1029/JB093iB05p04375.

Chouet, B. (1996), Long-period volcano seismicity: Its source and use in eruption forecasting, *Nature*, *380*(6572), 309–316, doi:10.1038/380309a0.

Chouet, B. (2003), Volcano seismology, *Pure Appl. Geophys.*, *160*(3–4), 739–788, doi:10.1007/978-3-0348-8010-7.13.

Chouet, B., G. Saccorotti, M. Martini, P. Dawson, G. De Luca, G. Milana, and R. Scarpa (1997), Source and path effects in the wave fields of tremor and explosions at Stromboli Volcano, Italy, *J. Geophys. Res.*, *102*(B7), 15,129–15,150, doi:10.1029/97JB00953.

Chouet, B., G. De Luca, G. Milana, P. Dawson, M. Martini, and R. Scarpa (1998), Shallow velocity structure of Stromboli Volcano, Italy, derived from small-aperture array measurements of Strombolian tremor, *Bull. Seismol. Soc. Am.*, *88*(3), 653–666.

Cigolini, C., A. Borgia, and L. Casertano (1984), Intra-crater activity, aa-block lava, viscosity and flow dynamics: Arenal Volcano, Costa Rica, *J. Volcanol. Geotherm. Res.*, *20*(1–2), 155–176, doi:10.1016/0377-0273(84)90072-6.

Cole, P. D., E. Fernandez, E. Duarte, and A. M. Duncan (2005), Explosive activity and generation mechanisms of pyroclastic flows at Arenal volcano, Costa Rica between 1987 and 2001, *Bull. Volcanol.*, *67*, 695–716, doi:10.1007/s00445-004-0402-6.

Davi, R., G. S. O'Brien, I. Lokmer, C. J. Bean, P. Lesage, and M. M. Mora (2010), Moment tensor inversion of explosive long period events recorded on Arenal volcano, Costa Rica, constrained by synthetic tests, *J. Volcanol. Geotherm. Res.*, *194*, 189–200, doi:10.1016/j.jvolgeores.2010.05.012.

Davi, R., G. S. O'Brien, L. D. Barros, I. Lokmer, C. J. Bean, P. Lesage, M. M. Mora, and G. J. Soto (2012), Seismic source mechanisms of tremor recorded on Arenal volcano, Costa Rica, retrieved by waveform inversion, *J. Volcanol. Geotherm. Res.*, *213*, 1–13, doi:10.1016/j.jvolgeores.2011.10.008.

Del Pezzo, E., M. La Rocca, and J. M. Ibáñez (1997), Observations of high-frequency scattered waves using dense arrays at Teide Volcano, *Bull. Seismol. Soc. Am.*, *87*(6), 1637–1647.

Di Lieto, B., G. Saccorotti, L. Zuccarello, M. La Rocca, and R. Scarpa (2007), Continuous tracking of volcanic tremor at Mount Etna, Italy, *Geophys. J. Int.*, *169*(2), 699–705, doi:10.1111/j.1365-246X.2007.03316.x.

Frankel, A., S. E. Hough, P. Friberg, and R. Busby (1991), Observations of Loma Prieta aftershocks from a dense array in Sunnyvale, California, *Bull. Seismol. Soc. Am.*, *81*(5), 1900–1922.

Garces, M. A., M. T. Hagerty, and S. Y. Schwartz (1998), Magma acoustics and time-varying melt properties at Arenal volcano, Costa Rica, *Geophys. Res. Lett.*, *25*, 2293–2296, doi:10.1029/98GL01511.

García-Yeguas, A., J. Almendros, R. Abella, and J. M. Ibáñez (2011), Quantitative analysis of seismic wave propagation anomalies in azimuth and apparent slowness at Deception Island volcano (Antarctica) using seismic arrays, *Geophys. J. Int.*, *184*, 801–815, doi:10.1111/j.1365-246X.2010.04864.x.

Goldstein, P., and R. J. Archuleta (1987), Array analysis of seismic signals, *Geophys. Res. Lett.*, *14*(1), 13–16, doi:10.1029/GL014i001p00013.

Goldstein, P., and R. J. Archuleta (1991), Deterministic frequency-wavenumber methods and direct measurements of rupture propagation during earthquakes using a dense array: Theory and methods, *J. Geophys. Res.*, *96*(B4), 6173–6185, doi:10.1029/90JB02123.

Goldstein, P., and B. Chouet (1994), Array measurements and modeling sources of shallow volcanic tremors at Kilauea Volcano, Hawaii, *J. Geophys. Res.*, *99*(B2), 2637–2652, doi:10.1029/93JB02639.

Gupta, I. N., C. S. Lynnes, T. W. McElfresh, and R. A. Wagner (1990), *F-K* analysis of NORESS array and single station data to identity sources of near-receiver and near-source scattering, *Bull. Seismol. Soc. Am.*, *80*(6), 2227–2241.

Hagerty, M. T., S. Y. Schwartz, M. A. Garces, and M. Protti (2000), Analysis of seismic and acoustic observations at Arenal Volcano, Costa Rica, 1995–1997, *J. Volcanol. Geotherm. Res.*, *101*(1–2), 27–65, doi:10.1016/S0377-0273(00)00162-1.

Haney, M. M. (2010), Location and mechanism of very long period tremor during the 2008 eruption of Okmok Volcano from interstation arrival times, *J. Geophys. Res.*, *115*, B00B05, doi:10.1029/2010JB007440.

Hung, H., and M. Kaveh (1988), Focussing matrices for coherent signal-subspace processing, *IEEE Trans. Acoust. Speech Signal Process.*, *36*(8), 1272–1281, doi:10.1109/29.1655.

Ibáñez, J. M., E. Carmona, J. Almendros, G. Saccorotti, E. Del Pezzo, M. Abril, and R. Ortiz (2003), The 1998–1999 seismic series at Deception Island volcano, Antarctica, *J. Volcanol. Geotherm. Res.*, *128*(1–3), 65–88, doi:10.1016/S0377-0273(03)00247-6.

Ibáñez, J. M., E. Del Pezzo, C. Bengoa, A. Caselli, G. Badi, and J. Almendros (2008), Volcanic tremor and local earthquakes at Copahue volcanic complex, Southern Andes, Argentina, *J. Volcanol. Geotherm. Res.*, *174*, 284–294, doi:10.1016/j.jvolgeores.2008.02.005.

Inza, L., J. Metaxian, J. Mars, C. Bean, G. O'Brien, O. Macedo, and D. Zandomeneghi (2014), Analysis of dynamics of vulcanian activity of Ubinas volcano, using multicomponent seismic antennas, *J. Volcanol. Geotherm. Res.*, *270*(0), 35–52, doi:10.1016/j.jvolgeores.2013.11.008.

Jousset, P., J. Neuberg, and S. Sturton (2003), Modelling the time-dependent frequency content of low-frequency volcanic earthquakes, *J. Volcanol. Geotherm. Res.*, *128*(1–3), 201–223, doi:10.1016/S0377-0273(03)00255-5.

Jurkevics, A. (1988), Polarization analysis of three-component array data, *Bull. Seismol. Soc. Am.*, *78*(5), 1725–1743.

Kawakatsu, H., and M. Yamamoto (2007), Volcano seismology, in *Treatise on Geophysics,* edited by G. Schubert, chap. 4.13, pp. 389–420, Elsevier, Amsterdam, doi:10.1016/B978-044452748-6.00073-0.

Konstantinou, K. I., and V. Schlindwein (2002), Nature, wavefield properties and source mechanism of volcanic tremor: A review, *J. Volcanol. Geotherm. Res.*, *119*(1–4), 161–187, doi:10.1016/S0377-0273(02)00311-6.

Kumagai, H., T. Saito, G. O'Brien, and T. Yamashina (2011), Characterization of scattered seismic wavefields simulated in heterogeneous media with topography, *J. Geophys. Res.*, *116*, B03308, doi:10.1029/2010JB007718.

La Rocca, M., E. Del Pezzo, M. Simini, R. Scarpa, and G. De Luca (2001), Array analysis of seismograms from explosive sources: Evidence for surface waves scattered at the main topographical features, *Bull. Seismol. Soc. Am.*, *91*(2), 219–231, doi:10.1785/0120000028.

La Rocca, M., G. Saccorotti, E. Del Pezzo, and J. Ibáñez (2004), Probabilistic source location of explosion quakes at Stromboli volcano estimated with double array data, *J. Volcanol. Geotherm. Res.*, *131*(1–2), 123–142, doi:10.1016/S0377-0273(03)00321-4.

Lesage, P., M. M. Mora, G. E. Alvarado, J. Pacheco, and J. P. Metaxian (2006), Complex behavior and source model of the tremor at Arenal volcano, Costa Rica, *J. Volcanol. Geotherm. Res.*, *157*, 49–59, doi:10.1016/j.jvolgeores.2006.03.047.

Lesage, P. (2009), Interactive Matlab software for the analysis of seismic volcanic signals, *Comput. Geosci.*, *35*, 2137–2144, doi:10.1016/j.cageo.2009.01.010.

Lindquist, K. G., I. M. Tibuleac, and R. A. Hansen (2007), A semiautomatic calibration method applied to a small-aperture Alaskan seismic array, *Bull. Seismol. Soc. Am.*, *97*(1B), 100–113, doi:10.1785/0120040119.

Lokmer, I., G. S. O'Brien, D. Stich, and C. J. Bean (2009), Time reversal imaging of synthetic volcanic tremor sources, *Geophys. Res. Lett.*, *36*, L12308, doi:10.1029/2009GL038178.

Matsumoto, S., H. Shimizu, T. Matsushima, K. Uehira, Y. Yamashita, M. Nakamoto, M. Miyazaki, and H. Chikura (2013), Short-term spatial change in a volcanic tremor source during the 2011 Kirishima eruption, *Earth Planets Space*, *65*(4), 323–329, doi:10.5047/eps.2012.09.002.

McNutt, S. R., and T. Nishimura (2008), Volcanic tremor during eruptions: Temporal characteristics, scaling and constraints on conduit size and processes, *J. Volcanol. Geotherm. Res.*, *178*(1), 10–18, doi:10.1016/j.jvolgeores.2008.03.010.

Melson, W. G., and R. Saenz (1968), The 1968 eruption of Volcán Arenal, Costa Rica: Preliminary summary of field and laboratory studies, *Tech. Rep. 7-1968*, Smithsonian Center for Short-Lived Phenomena, 35 pp.

Metaxian, J. P., P. Lesage, and J. Dorel (1997), Permanent tremor of Masaya volcano, Nicaragua: Wave field analysis and source location, *J. Geophys. Res.*, *102*(B2), 22,529–22,545, doi:10.1029/97JB01141.

Metaxian, J. P., P. Lesage, and B. Valette (2002), Locating sources of volcanic tremor and emergent events by seismic triangulation: Application to Arenal volcano, Costa Rica, *J. Geophys. Res.*, *107*(B10), 2243, doi:10.1029/2001JB000559.

Metaxian, J. P., G. S. O'Brien, C. J. Bean, B. Valette, and M. Mora (2009), Locating volcano-seismic signals in the presence of rough topography: Wave simulations on Arenal volcano, Costa Rica, *Geophys. J. Int.*, *179*, 1547–1557, doi:10.1111/j.1365-246X.2009.04364.x.

Minakami, T., S. Utibori, and S. Hiraga (1969), The 1968 eruption of Volcán Arenal, Costa Rica, *Bull. Earthquake Res. Inst. Tokyo*, *47*, 783–802.

Mora, M. (2003), Etude de la structure superficielle et de l'activité sismique du volcan Arenal, Costa Rica, PhD thesis, Université de Savoie, France.

Mora, M. M., P. Lesage, B. Valette, G. E. Alvarado, C. Leandro, J. P. Metaxian, and J. Dorel (2006), Shallow velocity structure and seismic site effects at Arenal volcano, Costa Rica, *J. Volcanol. Geotherm. Res.*, *152*, 121–139, doi:10.1016/j.jvolgeores.2005.09.013.

Neuberg, J., R. Luckett, B. Baptie, and K. Olsen (2000), Models of tremor and low-frequency earthquake swarms on Montserrat, *J. Volcanol. Geotherm. Res.*, *101*(1–2), 83–104, doi:10.1016/S0377-0273(00)00169-4.

Nisii, V., G. Saccorotti, and S. Nielsen (2007), Detailed analysis of wave propagation beneath the Campi Flegrei Caldera (Italy), *Bull. Seismol. Soc. Am.*, *97*, 440–456, doi:10.1785/0120050207.

O'Brien, G. S., and C. J. Bean (2004), A 3D discrete numerical elastic lattice method for seismic wave propagation in heterogeneous media with topography, *Geophys. Res. Lett.*, *31*(14), L14608, doi:10.1029/2004GL020069.

O'Brien, G. S., and C. J. Bean (2009), Volcano topography, structure and intrinsic attenuation: Their relative influences on a simulated 3D visco-elastic wavefield, *J. Volcanol. Geotherm. Res.*, *183*(1–2), 122–136, doi:10.1016/j.jvolgeores.2009.03.004.

Palo, M., J. M. Ibáñez, M. Cisneros, M. Bretón, E. Del Pezzo, E. Ocaña, J. Orozco-Rojas, and A. M. Posadas (2009), Analysis of the seismic wavefield properties of volcanic explosions at Volcan de Colima, Mexico: Insights into the source mechanism, *Geophys. J. Int.*, *177*, 1383–1398, doi:10.1111/j.1365-246X.2009.04134.x.

Patane, D., G. Di Grazia, A. Cannata, P. Montalto, and E. Boschi (2008), Shallow magma pathway geometry at Mt. Etna volcano, *Geochem. Geophys. Geosyst.*, *9*(12), Q12021, doi:10.1029/2008GC002131.

Rost, S., and C. Thomas (2002), Array seismology: Methods and applications, *Rev. Geophys.*, *40*(3), 2-1–2-27, doi:10.1029/2000RG000100.

Ryberg, T., C. Haberland, G. S. Fuis, W. L. Ellsworth, and D. R. Shelly (2010), Locating non-volcanic tremor along the San Andreas Fault using a multiple array source imaging technique, *Geophys. J. Int.*, *183*(3), 1485–1500, doi:10.1111/j.1365-246X.2010.04805.x.

Saccorotti, G., B. Chouet, and P. Dawson (2001), Wavefield properties of a shallow long-period event and tremor at Kilauea Volcano, Hawaii, *J. Volcanol. Geotherm. Res.*, *109*(1–3), 163–189, doi:10.1016/S0377-0273(00)00310-3.

Saccorotti, G., L. Zuccarello, E. Del Pezzo, J. M. Ibáñez, and S. Gresta (2004), Quantitative analysis of the tremor wavefield at Etna Volcano, Italy, *J. Volcanol. Geotherm. Res.*, *136*, 223–245, doi:10.1016/j.jvolgeores.2004.04.003.

Saccorotti, G., I. Lokmer, C. J. Bean, G. Di Grazia, and D. Patane (2007), Analysis of sustained long-period activity at Etna Volcano, Italy, *J. Volcanol. Geotherm. Res.*, *160*, 340–354, doi:10.1016/j.jvolgeores.2006.10.008.

Schmidt, R. (1986), Multiple emitter location and signal parameter estimation, *IEEE Trans. Antennas Propag.*, *34*(3), 276–280, doi:10.1109/TAP.1986.1143830.

Takagi, N., S. Kaneshima, H. Kawakatsu, M. Yamamoto, Y. Sudo, T. Ohkura, S. Yoshikawa, and T. Mori (2006), Apparent migration of tremor source synchronized with the change in the tremor amplitude observed at Aso volcano, Japan, *J. Volcanol. Geotherm. Res.*, *154*, 181–200, doi:10.1016/j.jvolgeores.2006.02.001.

Ueno, T., T. Maeda, K. Obara, Y. Asano, and T. Takeda (2010), Migration of low-frequency tremors revealed from multiple-array analyses in western Shikoku, Japan, *J. Geophys. Res.*, *115*, B00A26, doi:10.1029/2008JB006051.

Valade, S., F. Donnadieu, P. Lesage, M. M. Mora, A. Harris, and G. E. Alvarado (2012), Explosion mechanisms at Arenal volcano, Costa Rica: An interpretation from integration of seismic and Doppler radar data, *J. Geophys. Res.*, *117*, B01309, doi:10.1029/2011JB008623.

Wadge, G. (1983), The magma budget of Volcán Arenal, Costa Rica from 1968 to 1980, *J. Volcanol. Geotherm. Res.*, *19*(3–4), 281–302, doi:10.1016/0377-0273(83)90115-4.

Wadge, G., D. Oramas-Dorta, and P. D. Cole (2006), The magma budget of Volcán Arenal, Costa Rica from 1980 to 2004, *J. Volcanol. Geotherm. Res*, *157*, 60–74, doi:10.1016/j.jvolgeores.2006.03.037.

Williams-Jones, G., J. Stix, M. Heiligmann, J. Barquero, E. Fernandez, and E. D. Gonzalez (2001), A model of degassing and seismicity at Arenal volcano, Costa Rica, *J. Volcanol. Geotherm. Res.*, *108*(1–4), 121–139, doi:10.1016/S0377-0273(00)00281-X.